MODELING STACKING DISORDER IN SOIL KAOLINITE

A Thesis

by

BIDEMI TOKUNBO FASHINA

Submitted to the Office of Graduate and Professional Studies of
Texas A&M University
in partial fulfillment of the requirements for the degree of

MASTER OF SCIENCE

Chair of Committee,	Youjun Deng
Co-Chair of Committee,	Thomas Yancey
Committee Members,	Anil Somenahally
	Paul Schwab
Head of Department,	David Baltensperger

December 2018

Major Subject: Soil Science

ABSTRACT

Kaolinite is ubiquitous in soils and is the dominant clay mineral in highly weathered soils such as Oxisols and Ultisols. The determinative roles of mineral structures at the atomic level in their surface properties, their interactions with nutrients, contaminants, and biological compounds have been documented. Yet the structural details of clay minerals in soils are generally unknown or poorly characterized due to the complexity of mineral assemblage and often abundant structure disordering. In the past decades, there are ample studies on the nature (abundance and type) of structural disorder in geologic kaolinite, many computer programs have been developed to quantitatively describe the disordering. The objectives of this study were 1) to model disordering of soil kaolinite using the programs commonly employed in single-composition geological specimens, 2) to identify the factors or parameters limiting soil kaolinite structure modeling and the possible solutions for these limiting factors, and 3) to examine the effect of the disordering on the thermal stability of kaolinite.

Two pedogenic kaolinites, one from Brazil labeled BRZ and one from Hawaii label WAI were the focus of the study. One sedimentary kaolinite from Georgia labeled KGa was included for comparison and verification of accuracy of the modeling procedures.

The structural disorder was studied by modeling the X-ray diffraction (XRD) patterns of the samples using computer program FAULTS. The disorder model used assumes that a disorder-free kaolinite will be produced from a 1:1 sequence of either a B

layer (displacement vector $\vec{t}_1$) or its enantiomorph (displacement vector $\vec{t}_2$), while the random interstratification of the $\vec{t}_1$ and $\vec{t}_2$ vectors within the kaolinite structure causes disorder. A third layer displacement vector, $\vec{t}_0$, located along the empty B octahedral site may also exist. This model attempts to estimate *Pt₁*, *Pt₂* and *Pt₀* which are the proportions of $\vec{t}_1$, $\vec{t}_2$, and $\vec{t}_0$ layer displacement translations, respectively within the structure.

The modeling of the KGa kaolinite was only possible after using two phases — an almost no disorder phase (NDP) and a highly disordered phase (HDP) both having different *Pt₁*, *Pt₂* and *Pt₀*. The soil kaolinite samples were both modeled with single-phase and contained 43, 30 and 27% of a *Pt₁*, *Pt₂* and *Pt₀*, respectively. High XRD profile factor (Rp = 16 – 19%) observed for the soil samples was likely due to preferential orientation, accessory minerals and amorphous phases.

The major limiting factor in modeling disorder in soil kaolinite was the presence of crystalline and amorphous phases of other minerals which often share the same diffraction peaks as kaolinite.

Thermal dehydroxylation experiments showed that the least disordered sample (KGa) was most resilient to dehydroxylation while BRZ and WAI showed similar trends.

DEDICATION

Dedicated to all my Teachers.

ACKNOWLEDGEMENTS

I would like to thank my committee chair, Dr. Youjun Deng, and my committee members, Drs. Anil Somenahally, Thomas Yancey and Paul Schwab for their guidance throughout the duration of the research and the writing of this thesis.

Thank you to the members of the soil mineralogy group, Chun-Chun Hsu and Ana Barrientos, for their input during this study. A big thank you to my mother, sister and Biola for their support. Thank you Biola for being a shoulder to lean on those dark days when I felt stuck in my research. Thank you.

Finally, I thank God by whose grace I am what I am: and his grace which was bestowed upon me was not in vain.

CONTRIBUTORS AND FUNDING SOURCES

I acknowledge the support and contributions of my faculty chair — Dr. Youjun Deng and all committee members — Drs. Anil Somenahally, Thomas Yancey and Paul Schwab.

I will like to express my eternal gratitude to the Norman Borlaug Institute, Texas A&M for the Borlaug International Scholars Fellowship through which my degree was financially supported. Also, I am forever grateful to the Department of Soil and Crop Sciences for their financial support during the duration of my M.S degree program.

TABLE OF CONTENTS

Page

LIST OF FIGURES

Page

LIST OF TABLES

Page

1. INTRODUCTION

Kaolinite is a 1:1 layered silicate mineral of the kaolin subgroup formed from the weathering of feldspars, micas, or other aluminum silicate minerals, by hydrothermal activities, or as authigenic sedimentary mineral**.** Commercial kaolinite has important industrial uses such as in the filling and coating of paper, ceramics, paint, plastics (Murray, 1991). Though less importance, in terms of soil functionalities, when compared to 2:1 layer silicate minerals, kaolinite in soils contribute to the retention of anions and cations, reduction of mobility of toxic ions, and water retention in highly weathered soils.

Kaolinite consists of 1:1 dioctahedral layer structures with an ideal formula of $Al_2Si_2O_5(OH)_4$. Limited isomorphous substitution in both geological and soil kaolinites guarantees no or little deviation from this ideal chemical composition but common layer stacking disorder within the crystal structure leads to structural defects and hence significant deviation from the ideal structure. Stacking disorder is formed during crystal growth, during deformation or during polymorphic transformations (Veblen, 1985), allowing kaolin minerals to form polytypes and twins of diverse order/disorder (Zvyagin & Drits, 1996).

Stacking disorder in geological deposit kaolinites has been extensively studied mainly because it influences industrial applications (Chàvez & Johns, 1995) and geological interpretations (Ruiz Cruz, 1994) of the mineral. Since kaolinite occurs as fine particles, the most common and useful technique to study stacking disorder is powder X-ray diffraction (XRD) and transmission electron microscopy (TEM). The XRD patterns

of randomly oriented specimens can reveal the extent of order or disorder in kaolinites. Well-ordered kaolinites are characterized by sharp and narrow *hkl* peaks while those of disordered specimens show blurred and asymmetrical basal diffraction peaks (Brindley, 1980).

In the last ~70 years, the study of stacking disorder has taken two approaches — qualitative and quantitative. The work of Hinckley (1962) is a classic example, amongst others, of the qualitative approach. Hinckley and similar authors derived simple indexes (e.g. Hinckley Index) that were used as a measure of the degree of disordering. The major drawbacks of the developed indexes were that they were solely based on empirical concepts and not on real defect models and that they cannot be used to extract information on the types or diversity of disorder in kaolinite samples (Plancon & Zacharie, 1990). The quantitative method is based on fundamental concepts as it attempts to calculate (model) an XRD pattern using real disordered structural models. The calculated pattern is then compared with the experimental pattern to validate the model (Drits & Tchouba, 1990). With this approach it was possible to (a) investigate the type and abundances of stacking disorder in kaolinite samples and (b) uphold or refute certain proposed models for stacking disorder in kaolinites. Examples of proposed models include stacking disordering due to — $\pm \vec{b}/3$ displacements, 120º rotations, octahedral vacancy model, enantiomorphism, etc. (Drits & Tchoubar, 1990).

There is ample information on stacking disorder in geologic kaolinite samples, but to the best of our knowledge, no attempt has been made to describe stacking disorder in soil kaolinite. The most probable challenges of modeling structural disorder in soil

kaolinite includes (a) the small crystallite size of soil kaolinite, (b) high density of stacking disorder in soil kaolinites, and (c) the presence of additional, poorly crystalline minerals and amorphous phases in soils even within the clay fraction of kaolinite rich soils. To overcome the challenge posed by the presence of these other minerals, which will hereafter be referred to as accessory minerals, it is imperative to screen out these interfering minerals in the soil so as to have a good agreement between the calculated pattern and experimental XRD pattern.

The objectives of this study are to:

a) evaluate the best approach to be used to suppress the factors or parameters that interfere with structure modeling of soil kaolinite;
b) study both the abundance and type of stacking disorder in soil kaolinites by modeling the XRD patterns of soil kaolinite samples and;
c) investigate the influence of structural disorder on thermal stability of kaolinite.

2. LITERATURE REVIEW

2.1 Kaolinite

Kaolinite is the most abundant member of the kaolin subgroup of the 1:1 layer silicate minerals while other members are halloysite, dickite and nacrite. Kaolin minerals consist of 1:1 layers of combined di-octahedral and tetrahedral sheets, they have the same ideal formula of $Al_2Si_2O_5(OH)_4$. The members of the kaolin subgroup are actually polytypes of the same mineral differing only in stacking sequence of the layer, yet their individual names were recommended to be retained (Guggenheim et al., 1997).

The name "Kaolinite" is derived from the Chinese word 'kauling', which means high-ridge, as for many centuries kaolinite was mined on a high-ridge near Jauchou Fu, China. The mineral can be formed from geologic processes (such as sedimentary layering and erosion/deposition) and pedogenic (soil) processes such as illuviation, eluviation, bioturbation.

Besides being low cost, geologic kaolinite is useful in diverse applications owing to certain physical and chemical properties such as a white (or near-white) color, inertness over a wide pH range, fine particle size, low conductivity of heat and electricity, very low charge on the lattice (Murray, 2006). Examples of such application include coating and filling paper, as a pigment extender in water-based interior latex paint, ceramics, as a carrier for catalysts (Murray, 2006).

Kaolinite is ubiquitous in soils due to pedogenesis within the soil and/or inherited from kaolinitic parent materials (White & Dixon, 2002). Tropical and subtropical soils are

usually dominated by kaolinite in the clay fraction. These soils are often characterized by free drainage and intense weathering. A large portion of the world's population depends on these soils for food production (Figure 1).

These soils are strongly weathered, acidic and low in organic matter. Kaolinite and iron oxides dominate the clay fraction of the soil while quartz and a few resistant primary

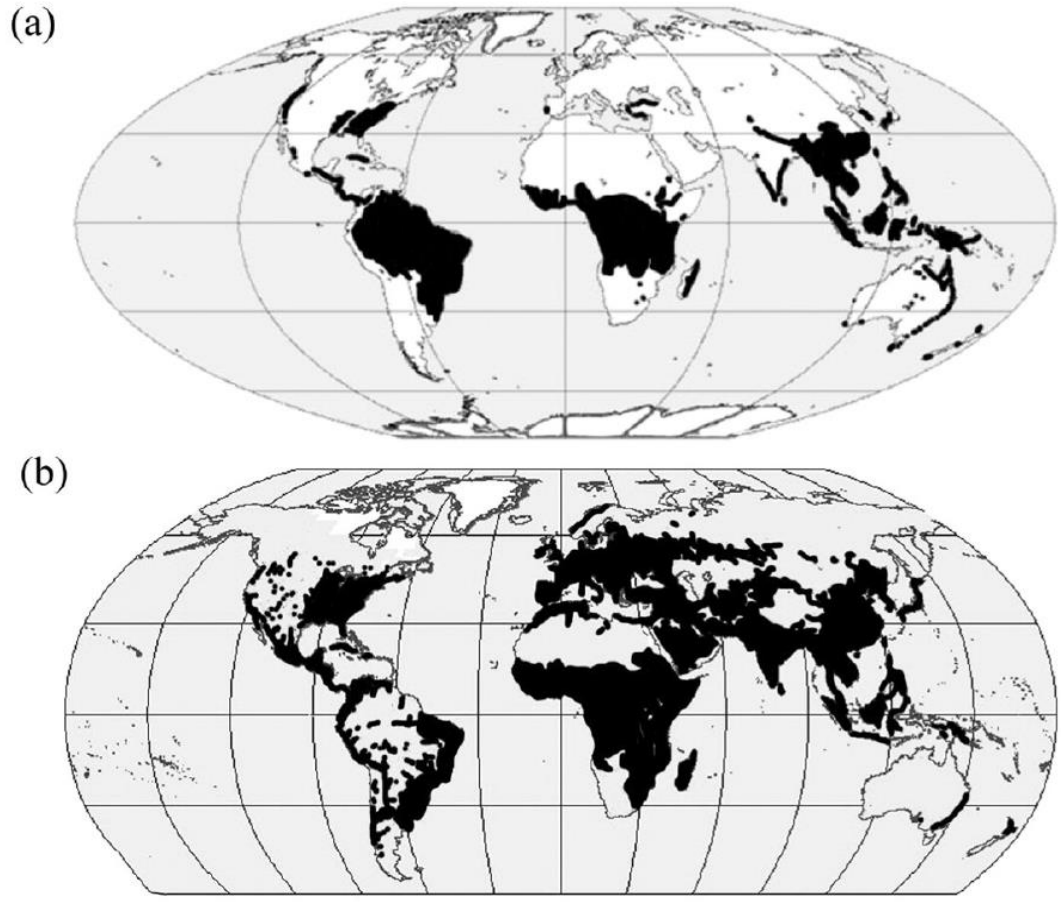

Figure 1. The global distribution of (a) kaolinite-dominated soils and (b) medium to high population density. Adapted from Gilkes & Prakongkep (2016)

minerals constitute the silt and sand fractions. Given these circumstances, these soils are characteristically poorly fertile, deficient in basic cations and high phosphorous fixation capacity — iron-phosphorus is dominant form of phosphorus. Despite being low in reactivity, functions of kaolinite in the soils include cation and anion retention, reduction of mobility of toxic ions, water retention, etc. (Gilkes & Prakongkep, 2016).

2.1.1 Composition and Structure

The members of the kaolin group have a nearly uniform composition of 46.3% SiO_2, 39.8% Al_2O_3 and 13.9% H_2O, which corresponds to an ideal formula $Al_2Si_2O_5(OH)_4$. Analyses of pure and well-crystallized commercial kaolinite samples show only small deviation from this ideal formula (Newman & Brown, 1987) which suggests that there is little to no substitution in the octahedral or tetrahedral sheets.

As a result of the possibility of little substitution, many kaolinites often contain only small amounts of Fe^{3+} (Meads & Malden, 1975) and Fe^{2+} (Pierre et al., 1992) within the octahedral sheet of the structure. As the content of Fe increases, structural order and crystal size decreases (Mestdagh et al., 1980; Singh & Gilkes, 1992). This substitution is very small in well crystallized kaolinite, but 1-3% Fe_2O_3 in poorly crystallized kaolinite and as high as 4% Fe_2O_3 in soil kaolinites (Wilson et al., 2013). For this reason, geologic kaolinites are better ordered in comparison to soil kaolinites. The latter often deviates from the ideal formula (46.3% SiO_2, 39.8% Al_2O_3 and 13.9% H_2O).

Accessory minerals (impurities) mostly found in kaolinite samples include small amounts of anatase, rutile, feldspar, iron oxides, mica, montmorillonite and quartz, all of

which must be corrected prior to estimating the extent (if any) of isomorphous substitution (Newman & Brown, 1987). These elements (Ti, K, Mg and Mn), occur in discrete impurity phases, or as surface-sorbed ions or complexes, and are not incorporated into the kaolinite structure (Lee et al., 1975; Weaver, 1976; Ma & Eggleton, 1999).

The fundamental unit in kaolinite is a single tetrahedral sheet and a single octahedral sheet, hence the classification of 1:1-layer silicate. The tetrahedral layer ($Si_4O_{10}^{4-}$) is formed by individual (SiO_4^{4-}) tetrahedron linked to neighboring tetrahedra by sharing three corners each, through the basal oxygens, to form a distorted hexagonal pattern with the unshared (apical) oxygens all pointing in the same direction normal to the sheet (Fig. 2a). The octahedral sheet in all kaolin members is formed by individual 6-fold coordination of aluminum by hydroxyls to give rise to an octahedron that is laterally linked to neighboring octahedron by sharing edges (Fig. 2b).

In kaolinites, two of the three octahedra positions are occupied by aluminum while the third octahedron is vacant (Fig. 2b), hence the classification dioctahedral. In cases, such as in serpentine minerals, where all the three positions are occupied mainly by divalent cations, the sheet is classified as trioctahedral. Going by Bailey's (1980) convention, the three non-equivalent sites are denoted as A, B and C. While, a 1:1 layer will be designated by a letter (B or C-layer) corresponding to the empty vacant site (Fig 2b). According to Bailey (1980), both B and C sites can be vacant thus giving rise to the possibility of two type of crystals containing B and C-layers that would have exactly the same XRD patterns. However, using a conventional unit cell ($\alpha > 90^o$ and $\gamma < 90^o$), refinements of kaolinite structure shows that the B site is always the vacant site (e.g.

Thompson & Cuff, 1985; Young & Hewat, 1988). For an ideal kaolinite ($\alpha = \gamma = 90^{o}$), Bailey's assumption would be correct. The angles α, β and γ being the angles between crystallographic axis "*b* and *c*", "*a* and *c*" and "*a* and *b*", respectively.

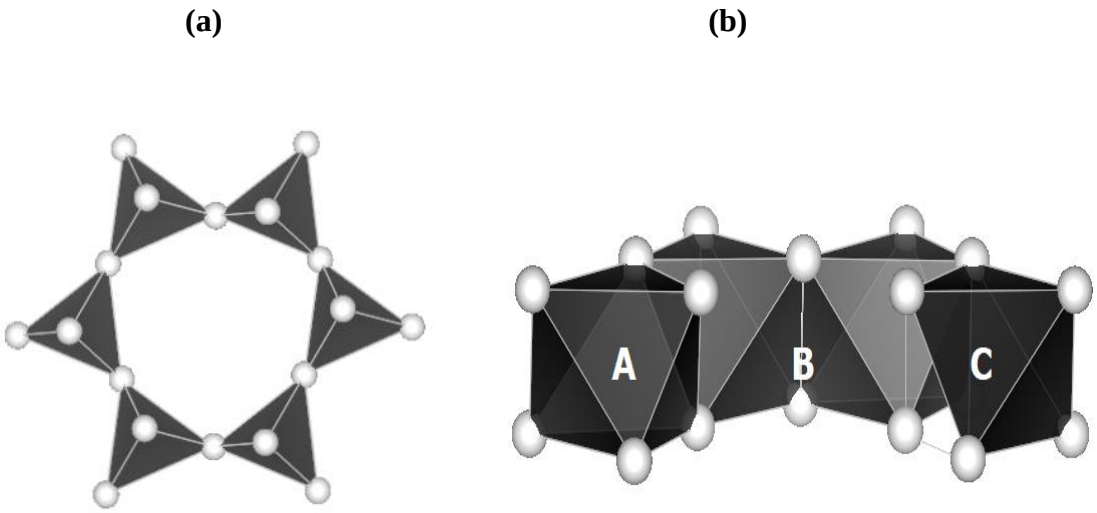

Figure 2 (a) The linking of Si—O tetrahedera to form six-membered hexagonal ring and (b) the linking of Al—OH octahedron having a vacant B octahedral site.

The linking of one tetrahedral sheet to one octahedral sheet (1:1 layer) is achieved by replacing two of every three oxygen anions of an octahedral sheet with the apical oxygen of the tetrahedral sheet. Thus, the outer plane of the aluminum octahedral plane consists of hydroxyls, outer plane of the silicon tetrahedral consists of oxygens and inner octahedral/tetrahedral plane consists of both hydroxyls and oxygens (Fig. 3).

The ideal tetrahedral sheet has a larger lateral dimension than the octahedral sheet. This mismatch is corrected by distortions such as tetrahedral rotations, tilting to form a network of ditrigonal rather than hexagonal symmetry, shortening of shared octahedral edges and counter rotation of the upper and lower triads of the octahedra (Wilson et al., 2013).

Adjacent 1:1 layers are stacked along the *c*-axis and are held together by long (~ 2.0 ± 0.10 Å) hydrogen bonds between the octahedral hydroxyls and tetrahedral oxygens (Fig. 3). In an ideal kaolinite, each adjacent layer is shifted by $-\vec{a}/3$ along the *a* axis such that the hydrogen bonds linking adjacent layers are approximately same length thus equalizing the interaction between the basal oxygen of the previous layer and the outer hydroxyl of the next layer (Brindley, 1961).

Several investigations have been conducted and differing conclusions have been reached about the orientation and position of the hydroxyl groups in kaolinite, especially the inner hydroxyls. The most common methods employed in these investigations were infrared (IR) and potential calculations. Hydrogen atoms scatter X-rays weakly and have incoherent scattering for neutrons thus making the location of hydrogen atoms difficult to locate in crystal structures by diffraction (Giese, 1988).

Though the recording of the IR spectrum of the hydroxyl groups is easy, getting structural information was difficult. This led to several conclusions with regards to the orientation of inner hydroxyls. Examples of conclusions reached about the orientation of the inner hydroxyl using data from IR includes that the inner hydroxyl is: perpendicular to the layer and directed towards the hexagonal opening formed by the six tetrahedra

(Serratosa et al., 1963; Wolf, 1963), oriented towards the empty octahedral site (Ledoux & White, 1964).

In view of the differing conclusions on the orientation of the inner hydroxyls using IR data, a different method needs to be explored. Baur (1965) and Ladd (1968) showed that in water molecules the hydrogen atoms are oriented such that electrostatic energy of the crystal is at minimum.

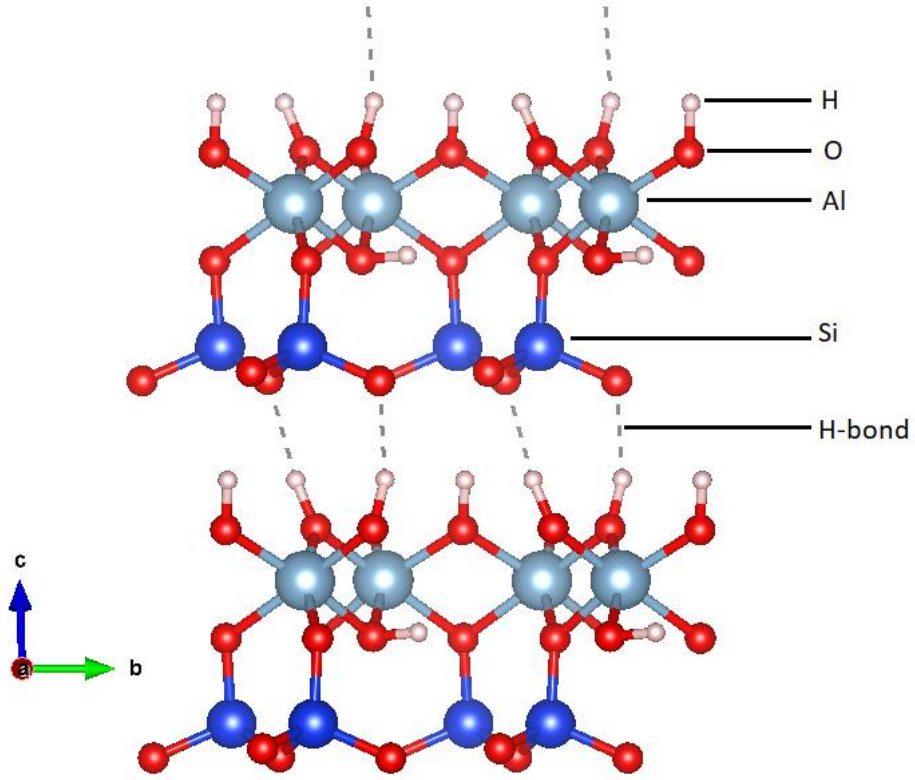

Figure 3 Ball-and-stick representation of kaolinite structure based on data by Bish and Von Dreele (1989). Unit layers are linked by hydrogen bonding between the octahedral hydroxyls and tetrahedral oxygens.

Since orientation corresponds to a potential minimum, it was possible to determine the orientation of the hydroxyl by calculating potential energy and ascertaining the minimum electrostatic energy. This approach resulted in determinations such as that the inner OH vector: is at an angle of 34º with the *001* plane (Adams, 1983), is directed alternately towards the tetrahedral and octahedral sheets (Young & Hewat, 1988), almost parallel to *001* plane (Bish, 1993) and makes an angle of 28º with the *001* plane in the direction of the tetrahedral sheet (Akiba et al., 1997).

Unlike the inner hydroxyls, there are not many discrepancies about the orientation of the surface hydroxyls. Ample studies have shown that for the surface hydroxyls to participate hydrogen bonding they have to be oriented almost perpendicular to the layers (Bish, 1993; Collins & Catlow, 1991; Young & Hewat, 1988).

The geometry of kaolinite unit cell was first reported as a 2-layered monoclinic cell (Gruner, 1932; Hendricks, 1936), but Brindley and Robinson (1946) found this to be incorrect since it was impossible to index the x-ray pattern of kaolinite using the postulated 2-layered monoclinic cell. Brindley & Robinson (1946) were able to index the XRD pattern of kaolinite using a 1-layered triclinic cell with a = 5.14 Å, b = 8.93 Å, c = 7.37 Å, $\alpha = 91.8^{\circ}$, $\beta = 104.5 - 105^{\circ}$ and $\gamma = 90^{\circ}$. The main difference from earlier 2-layered monoclinic cell approach was the c parameter which was approximately half of Gruner's value. Recent structure refinement of single crystal synchrotron data also confirmed that kaolinite has a *C1* symmetry with a = 5.154 Å, b = 8.942 Å, c = 7.401 Å, $\alpha = 91.69^{\circ}$, β = 104.61 and $\gamma = 89.82^{\circ}$ (Neder et al., 1999). These values are very similar to those obtained

through Rietveld refinement of neutron (D L Bish, 1993) and X-ray (Bish & Von Dreele, 1989) powder diffraction data.

2.1.2 Morphology

In general, there is great variation in terms of morphology of kaolin (Bates, 1971) even within a given deposit (Davis, 1950). Kaolinite occurs in variety of shapes such as euhedral, pseudo-hexagonal (most common) and platy. Geologic specimens are significantly larger and more regular in shape compared to soil kaolinite. Soil kaolinites seldom show hexagonal morphology; instead, the morphologies of irregular, sub-rounded to rounded, elongated plates are common (Hart et al., 2002; Melo et al., 2001; Singh & Gilkes, 1992). This is because only the basal faces are shown due to high degree of structural disorder (low crystallinity) and the eroding of non-basal faces by transport processes (White & Dixon, 2002). Large euhedral kaolin crystals have been seen in certain matured leached tropical soils; but, these kaolins are not pedogenic. Instead, they are inherited from deep regolith or sedimentary rocks soils (Varajão et al., 2001).

2.1.3 Surface Area

Measurement of surface properties (e.g. specific surface area) and bulk chemical properties of soil kaolin is difficult. This is because of the great diversity of minerals found in soils, even in kaolinite-dominated soils. Even the clay fractions of these soils contain accessory minerals (Hughes & Brown, 1979). Though chemical treatments can be applied to remove some impurities, such as Fe and Mn oxides, carbonates and organic matter, the

resulting mineral cannot be regarded to as pure kaolin (Gilkes & Prakongkep, 2016). Also, these treatments can influence certain measurements. For example, the removal of free Fe/Mn oxides is commonly achieved by digestion in dithionite-citrate-bicarbonate (DCB) solution but instead of removing just free Fe/Mn oxides, some structural Fe may be removed thus influencing the layer charge (Stucki, 2006). Rietveld refinement (H. Rietveld, 1969) is a less evasive approach through which quantification of clay minerals in clay fractions is possible and hence a reliable correction for impurities may be achieved.

Soil kaolin crystals are often very small and hence the specific surface area (SSA) and structural disorder are high. The high SSA allows for ionic retention which is important for agriculture since it guarantees the (a) retention of both cationic and anionic nutrients and (b) reduction of toxic ions that could contaminate crops and water bodies.

The SSA for soil kaolins is insensitive to the method used but depends upon the particle size of the individual sample (White & Dixon, 2002). Consequently there is a great variation in SSA values which could range from as low as 5 $m^2 g^{-1}$ (Dixon, 1989) to as high 90 $m^2 g^{-1}$ (Siradz, 2002). However, Gilkes & Prakongkep (2016) reviewed data from 13 publications on soil kaolin in tropical soils and concluded that SSA values in the range of 20-60 $m^2 g^{-1}$ is the most representative. Overall, soil kaolinites have higher SSA values and consequently higher chemical and physical reactivity compared to geologic specimens. SSA values typical of commercial deposits range from 8 to 12, 12 to 15 and 16 to 26 $m^2 g^{-1}$ for well-, medium- and poorly-crystalline kaolinite, respectively (Wilson et al., 2013).

2.1.4 Surface charge and exchange capacity

In ideal kaolinites, there is no substitution and the surface hydroxyl (from the octahedral sheet) and oxygens (from tetrahedral sheet) are fully charge-satisfied. Hence the mineral is regarded as being electrostatically neutral since no permanent charge is expected and both planar surfaces are relatively electrically neutral. However, there is possibility of a small negative permanent charge arising from the non-stochiometric substitution of Al^{3+} by Fe^{3+} or Fe^{2+} in the octahedral sheet (Meads & Malden, 1975; Pierre et al., 1992).

Kaolinites also have a variable (pH-dependent) net charge from unsatisfied bonds at multiple edges. Since the isoelectric point for kaolinite is pH 5.25 (Braggs et al., 1994), pH values higher than 5.25 kaolinite has a net negative charge while at pH lower than 5.25 the net charge becomes positive. The latter allows kaolinite to function as an important contributor to soil anion exchange capacity (AEC). Another mechanism for adsorbing anions on kaolinite is that of ligand exchange. Adsorption by ligand exchange is maximum near isoelectric point (Bergaya et al., 2006).

Reference kaolins typically have measurable CEC values between 0.4 and 5 cmol kg^{-1} (Hughes et al., 2009) while for soil kaolin values between 5 and 10 cmol kg^{-1} seem representative (Gilkes & Prakongkep, 2016). The latter authors attributed values outside of these range to errors that stems from presence of impurities and/or measurement. The influence of impurities is exemplified in the work by Lim et al. (1980) who found the CEC of Georgia kaolinites to be between 2.67 to 8.77 cmol kg^{-1} but after correcting for smectic

and micaceous impurities, the CEC of the pure kaolinite at pH 7 was from 0 to 1.0 cmol kg^{-1}.

2.2 Disorder in Clay Minerals

Crystals are constituted by periodically arranged atoms in 3-D space. This periodic configuration guarantees that the atoms of a crystals have long range repeated arrangement. A perfect crystal is one in which this periodic array of atoms is infinite in extent relative to the size of the repeating unit of structure. A disruption in this periodicity leads to disorder within the crystal structure. The recognition and evaluation of the extent and types of structural disorder are important for the identification of the mineral. Types of structural disorder includes thermal disorder, disorder in the distribution of cations, disorder in layer stacking, etc. (Brindley, 1980).

Thermal disorder arises from atomic thermal vibrations, always present in crystals, and represent a form of disorder whose contribution to entropy is well known (Rushbrooke, 1949). It reduces the intensities of X-ray diffraction peaks and the reduction increases with the angle of diffraction and temperature (Brindley, 1980).

Disorder because of distribution of cations is common in silicate minerals with isomorphous substitution. There is lack of true periodicity in the distribution of cations since there is tendency of equivalent points to be occupied by different kinds of atoms. For example, the size and/or charge difference that could arise from the isomorphous substitution of a cation for another leads to a small displacement of the atoms in the

disordered structure compared to the positions the atoms would have occupied in a perfect crystal (Drits & Tchoubar, 1990).

There is often more than one way to stack layers and hence the possibility of the formation of polytypes and loss of true periodicity, leading to structural disorder. Each stacking disorder modifies the relative position of the atoms located on both sides of the disorder (Drits & Tchoubar, 1990). This disruption in periodicity of the stacking of layers does not alter the chemistry of the mineral (Drits & Tchoubar, 1990) instead it affects properties of the minerals since these properties of minerals are a function of chemical and structural blueprints. For example, for kaolinites of geologic origin, stacking disorder has been shown to determine properties such as color, brightness, viscosity (Aparicio & Galan, 1999; Chàvez & Johns, 1995; Velho & de SF Gomes, 1991).

2.3 Assessment of Stacking Disorder in Kaolinite

Different methods such as XRD, selected-area electron diffraction (SAED), high resolution transmission electron microscopy (HRTEM) (Kogure & Inoue, 2005), small-angle X-ray scattering (SAXS) (Ben Rhaiem, 1999) and Fourier transmission infrared spectroscopy (FTIR) (Johnston et al., 2008) have been explored in the understanding of disordering in geologic kaolinites. Since kaolinite occurs as fine particles, powder XRD is the most convenient and common technique for studying stacking disorder in the mineral. The XRD patterns of well-ordered kaolinite have sharp and narrow *hkl* peaks while those of disordered specimens show blurred and asymmetrical basal reflections (Brindley, 1980). In extreme cases, peaks lose their identity and merge to form a two-

dimensional modulated band of diffracted intensity. Reflections where $k = 3n$ (where n is an integer) tend to be less affected than those of $k \neq 3n$.

Earlier XRD-based methods estimated the abundance of structural disorder in kaolinite as crystallinity index by calculating ratios of the intensities, above the background, of basal XRD diffraction peaks between 19º and 26º (Cu Kα radiation). Examples of tests based on this method are the (i) Hinckley index (HI) (Hinckley, 1962), Range–Weiss index (QF) (Range et al., 1969), Stoch index (IK) (Stoch, 1974) and Aparicio-Galán-Ferrell index (Aparicio et al., 1999). Hughes and Brown (1979) devised a crystallinity index for soil kaolinites since the measured reflections in earlier indices were often either absent or too weak in soil kaolinites. The major shortcoming of all these empirical approaches, was that they were qualitative. Hence the crystallinity indices only gave information about the extent of structural disorder in kaolinites but no information on the nature (e.g. types) of such disorder.

To remedy the shortcoming mentioned in the preceding paragraph, there is a need for detailed quantitative approaches that are based on actual disorder and could describe the nature (types and abundance) of disorder in kaolinites. This leads to the simulating of experimental XRD patterns based on disorder models. The accuracy of the disorder models from which calculated (modeled) patterns were derived is then assessed by evaluating how well the calculated XRD patterns reproduce experimental patterns. Disorder models whose diffraction pattern does not match the experimental data are considered inadequate to describe the real structure and are discarded (Drits & Tchoubar, 1990). The model that produces XRD pattern that best matches the experimental pattern

is retained. Proposed models for disorder and the evaluation of the accuracy of such models will be discussed in the next Section.

2.4 Causes of Stacking Disorder in Kaolinite

Several models have been proposed to describe the cause of stacking disorder in kaolinites. The leading models include stacking disordering due to: $\pm\vec{b}/3$ displacements between layers (Brindley & Robinson, 1946), 120º rotations (Murray, 1954), octahedral vacancy displacement, and enantiomorphism (Plançon & Tchoubar, 1977b). The governing force for the layers to align themselves in kaolinite is the paired H-bonding between the OH groups of octahedral sheet and the basal O in the neighbouring tetrahedral sheet (Fig. 3). More than 50 types of layer shifts or rotations can satisfy the pairing of the octahedral OH and tetrahedral O for H-bonding.

2.4.1 Stacking disorder due to displacements by $\pm\vec{b}/3$

Brindley and Robinson (1946) proposed that disordering is caused by random displacements of layers parallel to the *y*-axis by integral multiples of $\vec{b}/3$. The assumption was that since the OH ions in the external plane in ideal 1:1 layers are arranged at intervals of $\vec{b}/3$, any displacement of the layer by $p\vec{b}/3$ (*p* being integral) will result in the sheet of hydroxyl coinciding with itself after such additional displacements. This will result in the same H-bonding strength as in that without the displacement.

Plançon and Tchoubar (1975, 1977b) investigated the validity of this model by comparing calculated (modeled) patterns with actual experimental patterns of a highly order kaolinite from Georgia (USA) and highly disordered kaolinite from Charente district (France). The calculated patterns were generated by varying the proportion $\vec{b}/3$ and $-\vec{b}/3$ additional translations present in the structure alongside the $\vec{t}_0$ vector. Where $\vec{t}_0$ (approximately $-\vec{a}/3$) is the normal displacements between two adjacent layers. The diffractograms, generated by varying proportions of only $\vec{b}/3$ and $-\vec{b}/3$ translations, could not convincingly reproduce the experimental patterns of the samples. The nearest possible agreement between the calculated patterns and the experimental patterns is shown in Fig. 4 for *02l* and *11l* bands of the two samples based on P_T of 0.46 (Fig. 4 a) and 0.39 (Fig. 4 b) for the highly disordered and highly ordered sample, respectively, where P_T is the probability of occurrence of either $\vec{b}/3$ or $-\vec{b}/3$ translation disorders within the stack.

The inadequacy of this model stems from the $\vec{t}_0 - \vec{b}/3$ displacement leads to all the octahedral cations appearing exactly at the top of the Si of the adjacent layer (Bookin et al., 1989). The displacements $\vec{t}_0$ or $\vec{t}_0 + \vec{b}/3$ does not change the relative positions of the cations in the octahedral sheet of one layer and the cations in the tetrahedral sheet of the adjacent layer. The $\vec{t}_0 - \vec{b}/3$ displacement results in an arrangement that is electrostatically unfavorable and could only be found in "monoclinic kaolinite" which has yet to be documented in nature (Giese, 1988; Newman & Brown, 1987). An improvement on this

model would be to reduce or exclude the existence of such unfavorable stacking by reducing or excluding the probabilities of $\vec{t}_0 - \vec{b}/3$ displacement (Drits & Tchoubar, 1990).

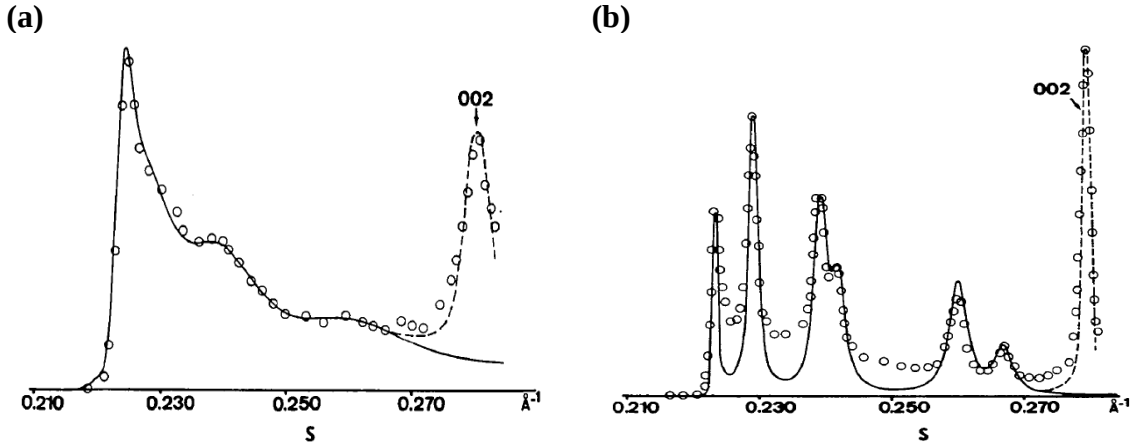

Figure 4 Experimental (circles) and calculated (line) patterns for (a) Charente and (b) Georgia kaolinites based on $\pm\vec{b}/3$ displacement model. Horizontal scale s = 2 sin θ/λ. Adapted from Plançon & Tchoubar (1975)

2.4.2 Stacking disorder due to ± 120° rotations

In this type of disorder, the interruption in the periodic arrangement of layers is attributed to irregular rotations of the layers in their own plane. The rotation model as proposed by Murray (1954) assumes that a ± 120° rotation by a layer results in the layer coinciding with itself except for the positions of the vacant octahedral site. Figure 5 can be used to show that the assumption on which the model is based on is not entirely correct. According to Bookin et al. (1989), the two-dimensional layer periodicity of defect-free

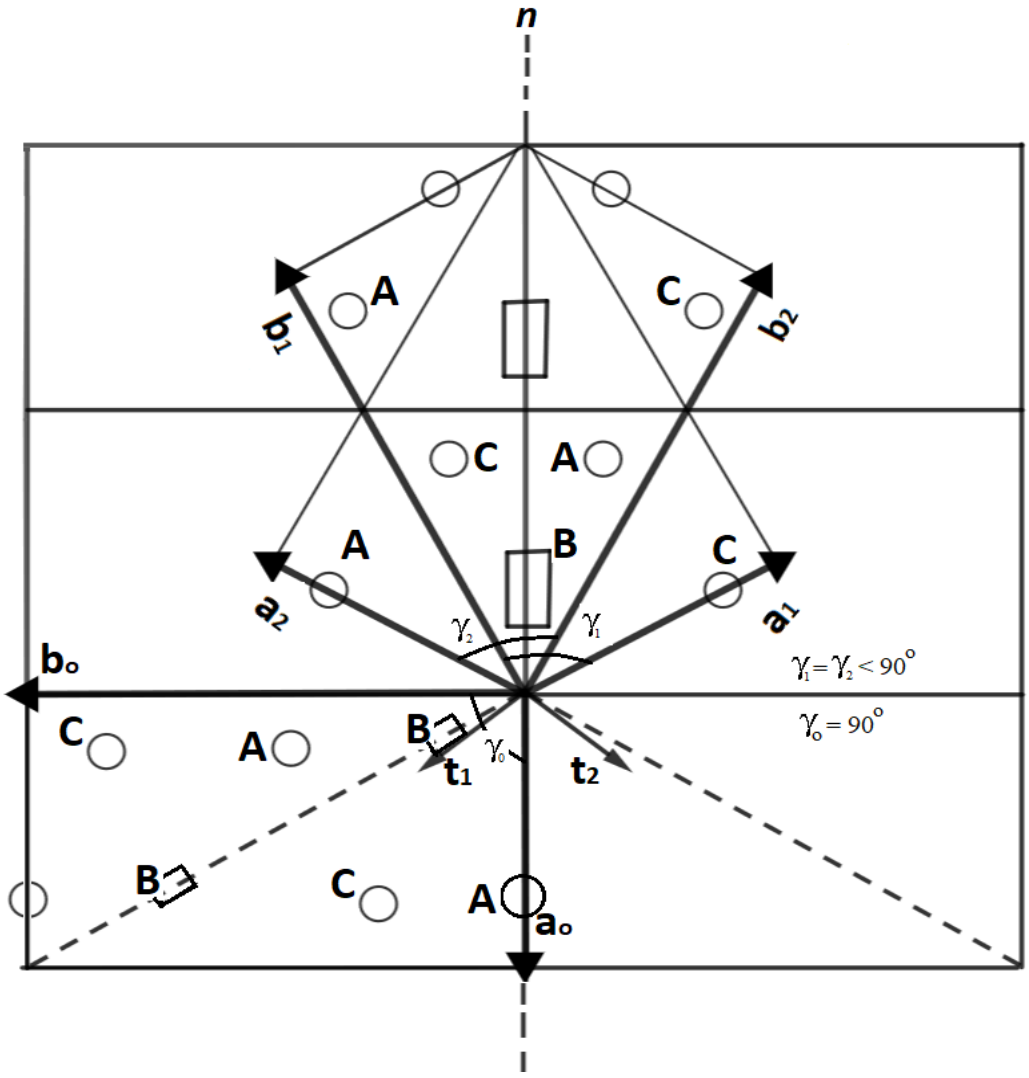

Figure 5. Possible unit cells for a dioctahedral 1: 1 layer depicting mutual arrangement of two oblique kaolinite-layer unit cells (i = 1, 2) related by a pseudo-mirror plane passing through the centers of vacant octahedra site. The two-layer displacements, $\vec{t}_1$ and $\vec{t}_2$, are related to the corresponding cells by the pseudo-mirror plane. The third kaolinite-layer unit cell (i = 0) is orthogonal. Adapted from Drits and Tchoubar (1990)

1TC kaolinite can be described equally well by three possible cells with the corresponding parameters a_i, b_i and γ_i (angle between *a* and *b*) (where $i = 0, 1, 2$) (Fig. 5). The first cell (a_0,b_0,γ_0) is an orthogonal cell with $\gamma_0 = 90°$ while the two other cells (a_1,b_1,γ_1) and (a_2,b_2,γ_2) are practically identical with $\gamma_1, \gamma_2 < 90°$. The two latter cells are related to each other by a mirror plane, i.e. enantimorphic, that passes through the vacant octahedral site and the center of the ditrigonal ring of the tetrahedral sheet in the kaolinite layer. The three sets would be equivalent in an ideal layer. By knowing the parameters of one cell, say a_i, b_i and γ_i, those of the other two cells can be calculated from Eq. (1):

$$4a_i^2 = a_1^2 + b_1^2 \pm 2a_1b_1 \cos\gamma_1$$
$$4b_i^2 = 9a_1^2 + b_1^2 \mp 6a_1b_1 \cos\gamma_1 \qquad (1)$$
$$\cos\gamma_i = (a_i^2 + b_i^2 - 4a_i^2)/2a_ib_i$$

where $i = 0, 2$.

The superscript in Eq. (1) corresponds to the cell (a_0,b_0,γ_0). The experimental ($i = 1$) and calculated ($i = 0, 2$) parameters for the Keokuk kaolinite are given in Table 1 (Bookin et al., 1989). From Table 1, sets (a_1,b_1,γ_1) and (a_2,b_2,γ_2) are identical (left- and right-handed unit cells), while the (a_0,b_0,γ_0) cell is practically orthogonal. This is a proof that although the lattice of a layer in kaolinite is not strictly hexagonal, it is not entirely asymmetric. After ± 120º rotation around the center of the hexagonal ring (Fig. 5), the basal oxygens in the ring occupy almost the same positions, but the centers of other rings no longer coincide. Since $\vec{a}_1$ and $\vec{a}_2$ are equal, a clockwise rotation will indeed result in the latter coinciding with the former, yet the angle of rotation is not 120º and the directions of $\vec{b}_1$ and $\vec{b}_2$ will differ by 0.4°, "so that the center of the hexagonal ring, which is separated by

Table 1. Periodicity of a 1:1 layer of regular Keokuk kaolinite

Parameters	i = 1	2	0
a	5.153	5.153	5.167
b	8.941	8.941	8.917
γ	89.82º	89.82º	90.00º
$(b/a)^2$	3.010	3.010	2.978

Adapted from Bookin et al. (1989)

about 18 Å (2 x b) from the axis of rotation, would shift by an additional 0.1 Å. It is only by violation of the periodicity of the layer that an important accumulation of this error can be avoided, but this would lead to very small coherent domains, in contradiction with the experimental data that these domains must be hundreds of Angstroms long" (Plançon & Tchoubar, 1977b; Tchoubaret al., 1982). By anti-clockwise rotation, $\vec{a}_1$ coincides in direction with $\vec{a}_0$ but the length is different, while $\vec{b}_1$ and $\vec{b}_0$ will not be parallel. Hence unless there is layer distortion, it will be impossible to describe both the original and rotated layers by a common lattice. Hence, the characterization of a disordering in kaolinite cannot be strictly based on concept of layer rotation. Using the ± 120° rotation model to generate calculated XRD pattern, it was impossible to reproduce the experimental XRD patterns of more or less disordered kaolinites (Artioli et al., 1995; Plançon & Tchoubar, 1976).

2.4.3 Stacking disorder due to octahedral vacancy displacement

To circumvent the difficulty in the above model (Section 2.4.2), Plançon and Tchoubar (1977b) proposed a model based on the assumption that a crystal are constituted by identically oriented layers in which any of the octahedral sites (A, B, or C) can be vacant for a given layer. Disorder-free B, C and A layers have translations $\vec{t}_0$, $\vec{t}_0 + \vec{b}/3$ and $\vec{t}_0 - \vec{b}/3$, respectively. Hence, each layer is associated with a given interlayer translation that coincides with or differs by ± b/3 from the defect-free translation in kaolinite. The parameters in this model are the proportion of each type of layer (A, B or C) and the probability of going from one type of layer to another. This model could not accurately produce a calculated XRD pattern that matches an experimental pattern. Based on this model, the calculated patterns could not account for the observed modulation of the (*02l*,*11l*) reflection seen in highly disordered kaolinite (Artioli et al., 1995). The shortcoming of the model was that it assumes an equal probability of occurrence (abundance) of the three kaolinite types (A, B and C) whereas only B-layers have been found in nature. Hence, "some of the defects introduced by Plançon and Tchoubar have a high energy (distortions of the layers, unfavorable stacking sequence, etc.) and therefore are unlikely in the low-energy environments where kaolinite typically forms" (Bookin et al., 1989). To avoid the formation of thick stacks of unfavorable layers, Tchoubar et al. (1982) adjusted their model by adding a set of variables to imply preference for B layers randomly alternating with A and C layers. The possible interlayer types thus increase, with B-C-B and B-A-B being most common. The B-C sequence of layers is stacking

sequence in dickite while the C-B and A-B stacking sequences correspond to monoclinic kaolinite (Bookin et al., 1989).

Bailey (1963) showed that kaolinite and dickite differ by the position of the vacant octahedral sites. The sequences in kaolinite is B-B-B-… while dickite is B-C-B-C-. Bailey proposed that the disorder in kaolinite can be attributed to random replacement of B-layers by C-layers. Bailey's model was investigated by Bookin using data published in Drits & Tchoubar (1990) by varying proportions of BC pairs and BB pairs. The proportion of BCpairs (W_{BC}) and BB pairs (W_{BB}) corresponding to dickite and kaolinite, respectively, was varied from between 0 and 1. As shown in Figure 6, the calculated XRD patterns derived from varying the proportions of kaolinite and dickite in the structure did not match experimental diffractograms of kaolinites. Also, electron microscopy has been used to show that growth steps in kaolinites are continuous terraces which indicate identical layers while dickite showed intersecting steps due to unequal growth rates (Samotoin, 1966). Kogure et al. (2010), however, found dickite-like disorder formed by C-B-C sequences in a kaolinite sample whose infrared spectrum had previously shown some dickite bands (Johnston et al., 2008).

2.4.4 Stacking disorder due to enantiomorphic B layers

In this model, stacking disorder in kaolinite is associated with crystal growth. It was formulated on the basis that in kaolinite layers, with respect to the *n* plane (Fig. 5), there is a symmetrical arrangement of atoms (Bookin et al., 1989). If $\vec{t}_1$ is assumed to be the translation between two consecutive B-layers then a disorder-free crystal is formed

when all the successive B-layers are displaced by the same vector $\vec{t}_1$. Disorder in the crystal will result when two consecutive layers are related by the pseudomirror plane *n* where *n* is a

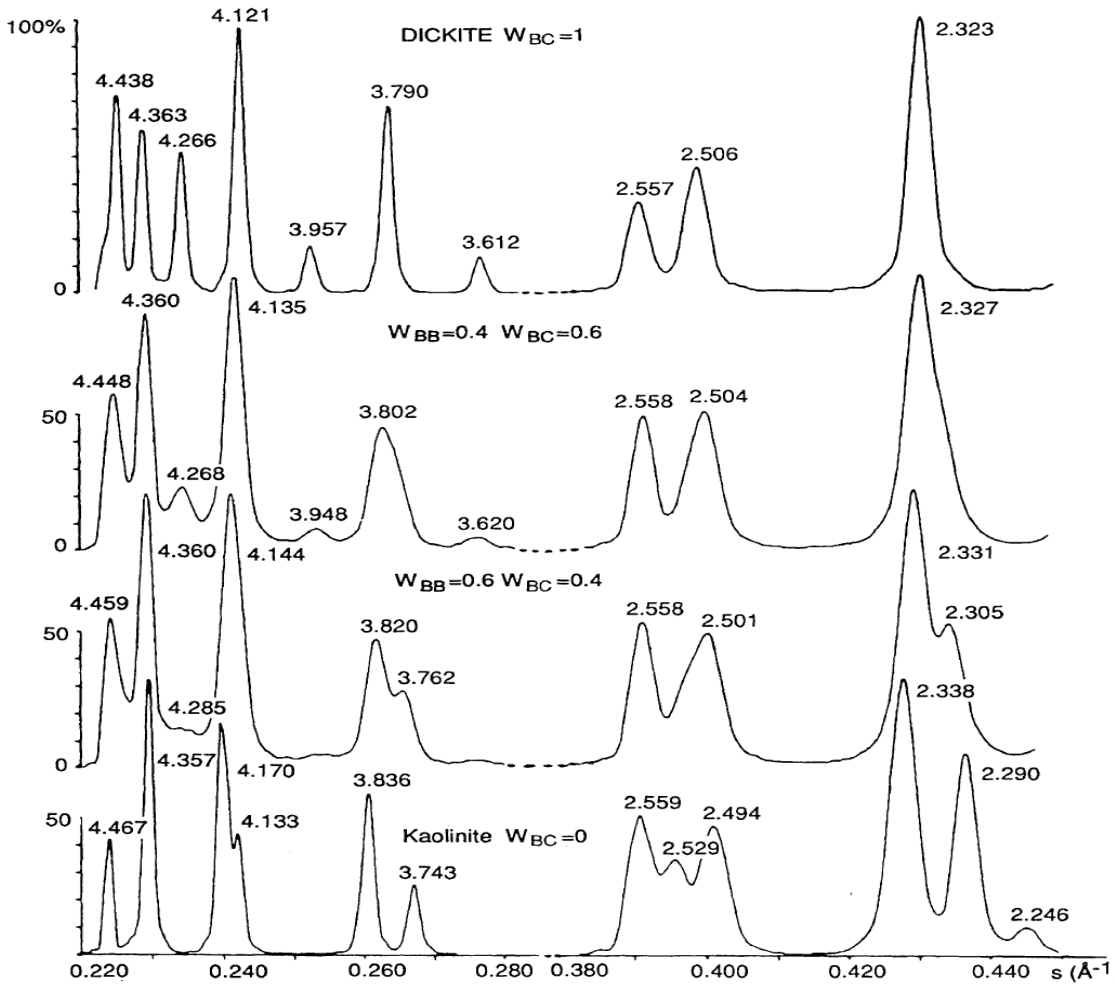

Figure 6 Calculated XRD patterns for kaolinite by varying the proportions of kaolinite (W_{BB}) and dickite (W_{BC}) within the structure. A $W_{BC} = 0$ (i.e $W_{BB} = 1$) will be equivalent to a pure kaolinite while $W_{BC} = 1$ (i.e $W_{BB} = 0$) is equivalent to pure dickite. Horizontal scale $s = 2 \sin \theta/\lambda$. Adapted from Drits & Tchoubar (1990)

a glide plane for the two layers. (Bookin et al., 1989). That is, disorder will be due to two adjacent layers being enantiomorphic. The disordered B-layer preserves the original periodicity and cation distribution formation with only small changes in the electrostatic energy of layer interaction and energy of the hydrogen bonding. The translation vector of the disordered layer is changed to $\vec{t}_2$ and it is related to $\vec{t}_1$ by the same glide plane *n* (see Fig. 5). The model of enantimorphic B-layers leads to alternating identical layers stacked with symmetrical translation vectors $\vec{t}_1$ and $\vec{t}_2$. Hence this model anticipates structural disorder because of the interstratification of the right-hand and left-hand structural fragments that consist of the same type of vacant layers.

Results from HRTEM studies have shown that the common source of stacking disorder in kaolinite are the alternation of alternative layer displacement vectors $\vec{t}_1$ and $\vec{t}_2$ (Kogure, 2011; Kogure et al., 2010; Kogure & Inoue, 2005).

Using the conventional (a_1, b_1, γ_1) system, the components of the projection $\vec{t}_1$ and $\vec{t}_2$ on the (*a*, *b*) plane are (- 0.369$\vec{a}_1$, - 0.024$\vec{b}_1$) and (-0.352$\vec{a}_1$, 0.304$\vec{b}_1$), respectively (Bookin et al., 1989).

The quantitative treatment of the model requires knowledge of these parameters: the short-range order factor (S = 1), the proportions W_i for the translation $\vec{t}_i$ and one of the probabilities α_{ij} (i,j = 1,2) of finding a translation $\vec{t}_j$ after the translation $\vec{t}_i$. The left- and right-handed unit cells of kaolinite being the same, two forms are equiprobable in a sufficiently large stack of crystallites, hence $W_1 = W_2 = 0.5$. All the P_{ij} can then be calculated if one of them, e.g. P_{11}, is known.

Shown in Figure 7 are simulated XRD patterns generated by varying P_{11} from 0 to 0.5 which corresponds to a change from ordered to random alternation of $\vec{t}_1$ and $\vec{t}_2$ and 0.5 to 1 (Fig. 8) corresponding to increasing segregation. Varying the values of P_{11} between 0 and 1 did not produce XRD patterns characteristic of some kaolinites. Most importantly, the model could not modify the intensities of the peaks at 19.8º (*020*) and 39.3º Cu Kα radiation (*013*) thus rendering the simulations incomparable to the (*020*) and (*013*) reflections of experimental patterns.

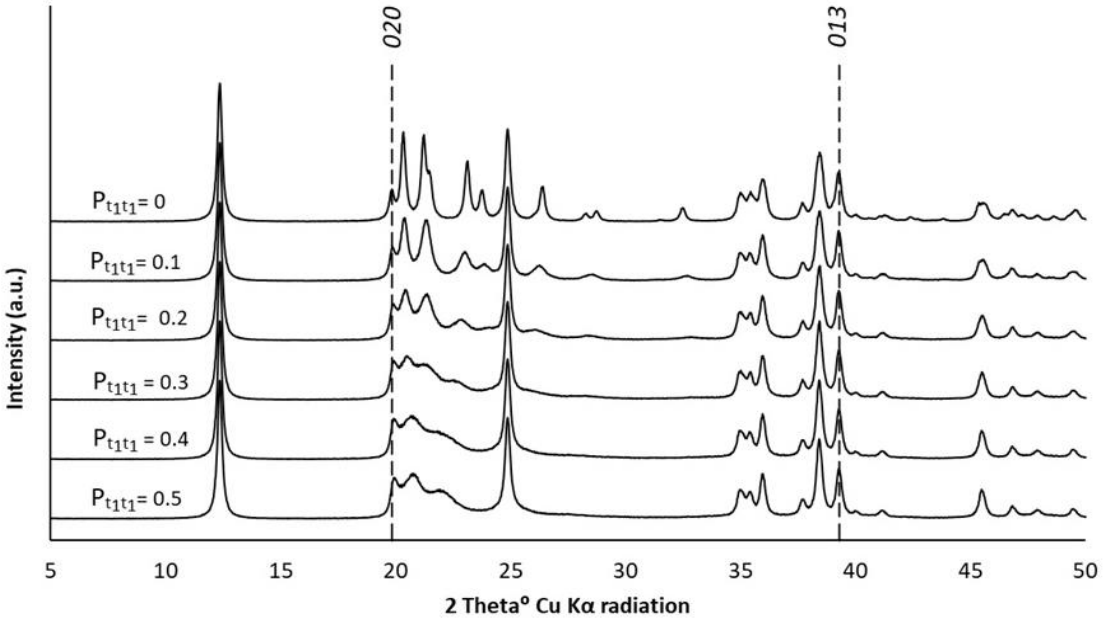

Figure 7 Calculated XRD patterns for single layer model of kaolinite. P_{T1T1}= 0 to 0.5

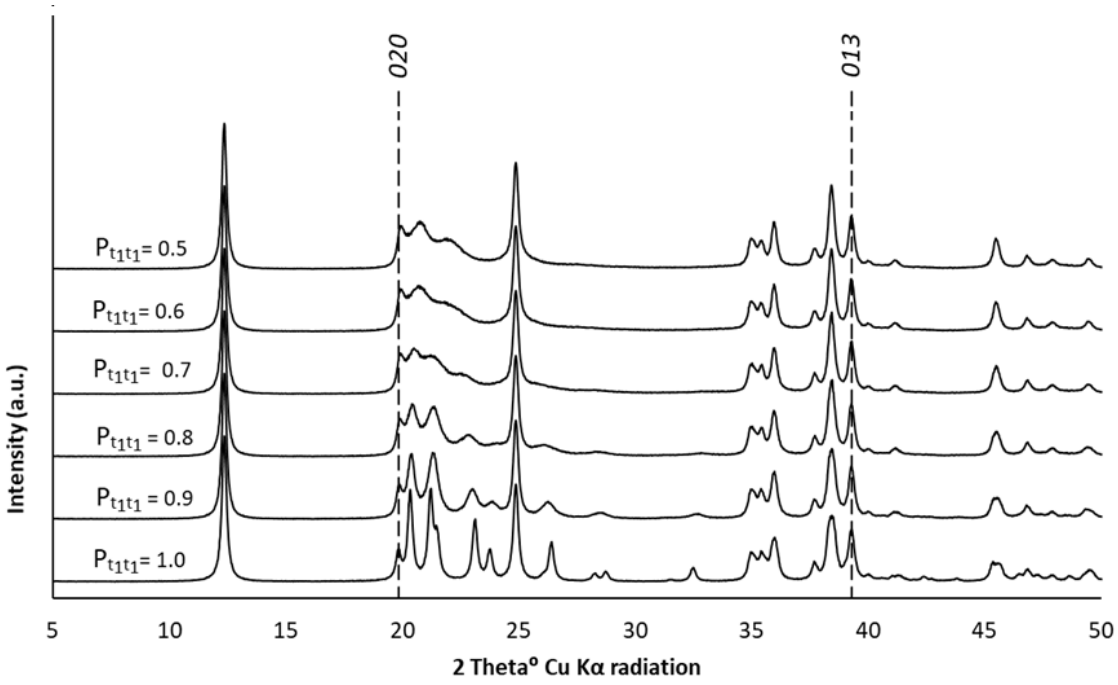

Figure 8 Calculated XRD patterns for single layer model of kaolinite. P_{T1T1}= 0.5 to 1

2.4.5 Stacking disorder due to enantiomorpbic B and some C layers

To overcome the shortcomings of the model containing only enantimorphic B-layers, Plançon & Tchoubar (1977a) introduced a "monoclinicity parameter" which slightly modifies α and β of the mean unit cell. A similar effect can be achieved by including a small proportion of C-layers (Drits & Tchoubar, 1990).

While the layer displacements $\vec{t}_1$ and $\vec{t}_2$ are related by a pseudo-mirror plane from defect-free 1Tc kaolinite enantiomorphs, another third layer displacement, $\vec{t}_0$, may exist. The $\vec{t}_0$ displacement is located along the long diagonal of the oblique layer unit cell that contains the vacant octahedral site and coincides with the layer pseudo-mirror plane (Fig. 5). In addition to these three-layer displacements, there could also be an additional

stacking disorder, $\vec{t}_a$, that displaces adjacent layers in arbitrary lengths and directions (Drits & Tchoubar, 1990). Thus, this model attempts to describe structural disorder in kaolinites by estimating the probability of $\vec{t}_1$, $\vec{t}_2$, $\vec{t}_0$ and $\vec{t}_a$ layer displacement translations $P\vec{t}_1$, $P\vec{t}_2$, $P\vec{t}_0$, and $P\vec{t}_a$ respectively, as determined by simulated experimental XRD patterns. Based on this model, (Plançon et al., 1989) successfully simulated a set of experimental XRD patterns of natural kaolinite samples and showed that some samples consist of a physical mixture of two distinct kaolinite phases. Sakharov et al. (2016) investigated the maximum proportion of the $\vec{t}_0$ layer displacement translations that could exist in a kaolinite structure and concluded that above 5% leads to significant shift in the positions of the *02l* and *11l* reflections in the simulated XRD pattern thus rendering such pattern incomparable to the experimental pattern.

2.5 Stacking Disorder in Soil Kaolinite

By exploring the modeling approach, several kaolinites of geologic origin have been studied (Artioli et al., 1995; Plançon & Tchoubar, 1977b; Sakharov et al., 2016). Unfortunately, this approach has not been extended to soil kaolinites. The most probable reasons why disordering in soil kaolinites has not been studied includes (a) non-industrial importance of soil kaolinites (b) small crystallite size of soil kaolinites, (c) high density of stacking disordering in soil kaolinites and (d) presence of additional minerals in soils.

The earliest studies of stacking disorder in kaolinites were to understand how such structural disorder affects the properties and application of the mineral, it is

understandable why disordering in pedogenic soil kaolinite has not been undertaken since pedogenic kaolinites have no industrial-application, neither do they (kaolinite) have profound effect on the soil property.

Pedogenic kaolinites are characterized by small crystallite size as well as high density (degree) of stacking disorder. Both can be readily inferred from the XRD patterns of kaolinite-dominated soils in which the *00l* reflections are usually broad and several other peaks are either absent or smeared. The absent, smearing and poor resolution of many peaks makes the simulation of the XRD patterns of soil kaolinites tedious.

The most significant technical reason for the lack of interest in the modeling of stacking disorder in soil kaolinites is the presence of other minerals (crystalline and amorphous phases) in kaolinite-dominated soils which makes the modeling challenging. The crystalline phases of these accessory minerals often share reflections with kaolinite while their amorphous phases lead to poor resolution of reflections. Hence, modeling of the primary mineral (kaolinite) would require methods that correct for the influence of both the accessory minerals and amorphous phases.

2.6 Approaches of Minimizing Interferences by Accessory Minerals

An approach to minimize the influence of the accessory mineral would be to use the clay fractions of these soils, but unfortunately, even the clay fractions of kaolinite-dominated soils often contain significant quantities of the accessory minerals.

Another approach would be to concentrate the kaolinite by selective dissolution and extraction of accessory minerals in the sample. This is also not an easy approach

because there is no absolute guarantee that such dissolution will (a) not affect the structural properties of kaolinite or (b) completely extract the accessory mineral(s). Also, there are scenarios where, there are no possible methods of separating the accessory mineral(s) from the primary mineral of interest.

A less-destructive approach is to quantify the accessory minerals and amorphous phases using the Rietveld approach (Rietveld, 1967; Rietveld, 1969; Bish & Post, 1993) and then masking the intensities of the reflections of the accessory minerals such that a fairly-pure experimental XRD pattern of kaolinite sample is obtained. The Rietveld method is used for the quantification of minerals contained in a given sample using the experimental XRD pattern of the sample. By using high quality structure models, the method attempts to estimate the contribution of each constituent mineral in the sample to the total experimental XRD pattern by simulating (calculating) the correct peak positions, shape and intensities of the reflections from individual minerals. Taking into account the ideal structure models, instrumental factors and specimen properties, the Rietveld method produces a calculated XRD pattern (y_{ic}) at *i*th step (2θ) as follows:

$$y_{ic} = S\sum_{K} L_K \left|F_K\right|^2 \phi(2\theta_i - 2\theta_K)\,\mathrm{P}_K\mathrm{A} + y_{bi}$$

where ***S*** is the scale factor — used to adjust the relative contribution of individual minerals to the overall experimental pattern, ***K*** is Miller indices (*h,k,l*) for a Bragg reflection, $\boldsymbol{L_K}$ contains the Lorentz-polarization and multiplicity factors — the polarization factor accounts for the intensity loss after the emitted x-rays are reflected by the monochromator crystal and on the sample prior to being acquired by the detector (Guinier, 1964), $\boldsymbol{F_K}$ is

the structure factor for the *K*th Bragg reflection, $\boldsymbol{\varphi\ (2\Theta_i - 2\Theta_k)}$ is the reflection profile (peak shape) function — estimates the effects of instrumental and specimen features, $\boldsymbol{P_K}$ is the preferred orientation function — to account for the anisotropic spatial, instead of random, orientation of the particles in the sample, **A** is the absorption factor — corrects for absorption of the X-rays as they pass through the irradiated volume of the specimen, and the $\boldsymbol{y_{bi}}$ is the background intensity at the *i*th step. The Rietveld approach minimizes **R** (error) by performing a least-square refinement (step-by-step) until a best-fit is obtained between the calculated pattern (y_i) and experimental (y_{ic}) XRD. The **R** is the sum of weighted (w_i) and squared differences between y_i and y_{ic} at *i*th step (2θ) in an XRD pattern.

$$R = \sum_i w_i \left| y_i - y_{ic} \right|^2$$

The minimum ***R*** can be obtained by adjusting the parameters that determine the y_{ic} using Rietveld refinement programs such as Topas (Coelho, 2005), Profex (Doebelin & Kleeberg, 2015), and SIROQUANT (Taylor, 1991). Since, the Rietveld method was originally developed for quantification of crystalline structures it was not immediately possible to use same method for the quantification of clay minerals. This is because of (a) the high degree of peak overlaps in the XRD patterns of clay minerals and (b) the lack of ideal structural models for clay minerals due to the complexity of structure that often arise due to varying degree of structural disorder. Yet the Rietveld method has been improved, with some degree of reliability, for the quantification of clay minerals in soils (Bish, 1994; Alves *et al*., 2007; Zabala *et al*., 2007; Brinatti *et al*., 2010).

3. MATERIALS AND METHODS

3.1 Sample Collection and Preparation

Two soil samples and one geologic kaolinite were used for the study. The first soil sample, labelled WAI (Tropeptic Eutrustox), was collected between 85 - 95 cm at the Poamoho Research Station, University of Hawaii. The second sample, labeled BRZ, was collected between 40 - 75 cm of an Oxisol at Acre state, Brazil. The BRZ is formed from fluvial-lacustrine sediments (Delarmelinda et al., 2017). Lastly, a cretaceous sedimentary kaolinite was collected at Arcilla mine, Georgia and labeled KGa. The samples were air-dried, gently crushed in a mortar then passed through a 2-mm sieve.

3.2 Size Fractionation

To facilitate the separation of the different size constituents, the samples were first pretreated to remove cementing and flocculating agents that could the binding individual particles. pH 5 sodium acetate (NaOAc) buffer solution was used to remove carbonate minerals while 30% hydrogen peroxide (H_2O_2) was used to remove organic matter. Iron oxides were removed by the dithionite-citrate-bicarbonate (DCB) method (Mehra & Jackson, 1960). The pretreated samples were then suspended in a diluted pH 10 Na_2CO_3 solution followed by separation of the sand fraction (> 53 µm) by sieving, while the silt fraction (2 – 53 µm) was separated from the clay fraction (> 53 µm) by centrifugation. To investigate the existence of multiple phases in KGa the silt and clay fraction (< 53 µm) was further separated into smaller sized particles (20 – 50, 10 – 20, 5 – 10, 2 – 5, 1 – 2,

0.5 – 1, 0.2 – 0.5, and < 0.2 μm) by sedimentation and centrifugation methods following guidelines described in Soukup (2008).

3.3 Electron Microscopy

The morphology and chemical composition of the minerals contained in the samples were studied by scanning electron microscope (SEM) and transmission electron microscope (TEM) equipped with X-ray Energy Dispersive Spectroscopy (EDS). The former being different from the latter in that it converts secondary electron signals (generated when a highly focused electron beam scans the surface of the sample) to electrical signals that are then converted to an image. While in the TEM, the focused electron beam passes through a specimen and two-dimensional image is generated (Deng, White, & Dixon, 2013). These microscopes are equipped with X-ray energy dispersive spectrometers (EDS) which gives the chemical composition of the observed particle and therefore can be used to identify the mineral contained in a given sample.

Samples for SEM were prepared, for KGa and WAI, by adding a drop of silt suspension into a vial containing distilled water to give a slightly turbid appearance. A drop of the turbid solution was transferred unto a double-sided carbon tab on a SEM stub and kept under a heating lamp to evaporate the water. A FEI Quanta 600 FEI QUANTA 600F field emission scanning electron microscope was used for SEM analysis.

In preparing the TEM samples for the clay fractions of WAI and BRZ, a few drops of a turbid clay suspension were taken and placed on a Cu metal grid that has been coated with a holey carbon film and left to dry under a heating lamp.

3.4 Spray-drying of Samples

A fundamental assumption in quantitative and structure XRD analysis is that the particles in the powder are entirely randomly oriented. In reality, the particles of many materials, especially clay minerals, tend to display preferential orientation. This deviation from the assumption leads to the modifications of both relative intensities and of the profiles of the XRD pattern diffraction peaks thus rendering the calculated patterns from quantitative or structural studies less reliable. To circumvent this, it is important to account for the influence of preferentially oriented particles on the intensities of experimental diffraction patterns or prepare powder XRD specimens that are fully randomly oriented. The former can be achieved in some Rietveld refinement programs and the latter through techniques such as spray-drying (Hillier, 1999; Smith et al., 1978). The spray-drying approach attempts to minimize or eliminate preferential orientation by spraying a suspension of the sample into a heated chamber so that it dries to form spherical aggregates of approximately uniform particle size and shape with random orientation.

The spray-drying procedure was conducted using Hillier's (1999) improved version of Smith et al. (1978) approach. Briefly, the sample was suspended in 0.5 % (w/v) aqueous solution of polyvinyl alcohol (PVA) and milled in a micronizing mill for 5 minutes at 3500 rpm. The slurry suspension was sprayed using a Badger artist's air brush that is connected to an air pump and to the sample slurry by tubing. The slurry is then sprayed as fine mist into a preheated (about 130 °C) aluminum chamber (Figure 9). The dried spherical aggregates were then collected on a white sheet of paper on the floor of

the chamber. Prior to XRD analysis, the spherical morphology of the aggregates was then confirmed using a light microscope at 6 X magnification.

Figure 9 Aluminum chamber and air-brush used in the spray-drying procedure

3.5 Experimental XRD Patterns

Experimental patterns to be modeled were acquired for the pretreated bulk KGa and the clay fraction of BRZ and WAI. The choice of clay fraction for BRZ and WAI was to reduce interferences from accessory minerals present in the sample. Influence of accessory minerals on the modeling of KGa is expected to be minimal since geologic specimens are pure in comparison to soil kaolinite. All samples were side-loaded, and the XRD patterns were acquired on a Bruker D8 diffractometer (40 kV, 40 mA, Bragg-Brentano mode with 250 mm goniometer radius) with CuKα radiation, a step/scan mode with 0.02°2θ step increment with a 20 s dwell time at each step and a 5-70°2θ range.

3.6 Approaches of Minimizing Interferences by Accessory Minerals

As earlier discussed in section 2.5, the significant presence of additional minerals (crystalline and/or amorphous phases) in the studied samples would lead to difficulty in the modeling of kaolinite disordering in such sample thus leading to poor agreement between the experimental and calculated pattern. This problem is especially expected for BRZ and WAI since both samples are of pedogenic origin. The approaches to solving the were (a) thermal destruction and (b) quantification of accessory minerals by Rietveld refinement.

3.6.1 Thermal destruction of accessory minerals

The rationale behind the approach was to explore the differences in the thermal stability of the minerals in the sample. The sample is heated at several designated

temperatures and XRD pattern is acquired for each temperature of interest. The goal is, through simple mathematics, to generate a pure XRD pattern for kaolinite and the accessory minerals in each sample.

For WAI, the XRD pattern of the original sample was acquired at room temperature and labeled *R*. The same sample was heated in a furnace at 300 °C for one 1 hour to destroy gibbsite and the XRD pattern was again acquired and labeled *T*. Finally, the WAI labeled *T* was heated at 550 °C for 1 hour to destroy kaolinite leaving behind a XRD pattern labeled *F* which represents other accessory minerals like mica, quartz, anatase and rutile, since these minerals are stable at 550 °C. To generate XRD pattern for kaolinite in the sample the following formulas were employed:

R – T = G

R – F = KG

R – G = KA

R – G – F = K

Where R = XRD pattern of the sample at room temperature

T = XRD pattern of the sample at 300 °C

G = XRD pattern of the gibbsite (one of the accessory minerals)

F = XRD pattern of the sample at 550 °C

KG = XRD pattern of the kaolinite and other accessory minerals

KG = XRD pattern of the kaolinite and gibbsite

K = XRD pattern for kaolinite (free off accessory minerals)

3.6.2 Rietveld refinement

Using the Rietveld approach, as discussed in section 2.6, the accessory minerals were quantified using refinement program — Profex (Doebelin & Kleeberg, 2015).

3.7 Calculated XRD Patterns

3.7.1 Simulation and refinement of calculated XRD patterns

The simulation and refinement of the XRD patterns was conducted with program FAULTS (Casas-Cabanas et al., 2016), which allows for simulation and refinement of the XRD and Neutron Powder Diffraction (NPD) patterns of crystal systems with any type of coherent planar disorder (defect). FAULTS uses a rigorous recursive approach to generate random stacking sequences modeling the presence of disordering. The method exploits the recurring stacking sequences observed in random stacking sequences to compute the average interference wavefunction scattered from each layer type occurring in a faulted crystal. The mathematical details entailed can be found in Treacy et al. (2010) and Hendricks (1942). Briefly, to simulate disorder, stacking is described in terms of the probability matrix α of order n, where n is the number of distinct layers (transition matrix). Each element, α_{ij}, refers to the probability of stacking layer *j* over layer *i* in the sequence. As an example, consider a crystal consisting of three crystallographically different layers (1, 2, and 3) having a probability matrix:

$$\alpha = \begin{pmatrix} \alpha_{11} & \alpha_{12} & \alpha_{13} \\ \alpha_{21} & \alpha_{22} & \alpha_{23} \\ \alpha_{31} & \alpha_{32} & \alpha_{33} \end{pmatrix}$$

Where the probability of layer 1 to be followed by 1, 2 or 3 layer is α_{11}, α_{12} or α_{13}, respectively. Since the values of α_{ij} can be controlled, the total density of disorder, type of disorder and their proportions can be evaluated in structure.

The quality of the agreement between observed and calculated profiles is given by the R-Factor (Rp) and Chi^2 agreement factors that are calculated at the end of each refinement cycle and are defined as follows:

Profile factor:
$$Rp = 100 \frac{\sum_{i=1,n} |y_i - y_{ic}|}{\sum_{i=1,n} y_i}$$

where y_i is the experimental (observed) intensity and y_{ic} is the calculated intensity at the *ith* step.

Reduced Chi square:
$$Chi^2 = \left[\frac{R_{wp}}{R_{exp}} \right]^2$$

where R_{wp} and R_{exp} are the Weighted Profile Factor and the Expected Weighted Profile Factor respectively. The lower the value of Rp, the higher the degree of agreement between the calculated and experimental XRD pattern.

Due to the significant presence of other minerals alongside kaolinite in the soil samples, unlike the geologic sample, it was necessary to quantify and block other phases that are contained in the samples alongside with kaolinite. This is important to avoid the

interference of other minerals with the modeling of stacking disorder in kaolinite. The XRD patterns of the accessory minerals contained in the original XRD patterns of the soil samples were estimated using Profex, imported into FAULT as background XRD patterns and blocked prior to simulation of structural disorder in the samples.

3.7.2 Model

The stacking disorder model used in the generating the calculated patterns was the enantiomorpbic B and some C layers as described in section 2.4.5. Briefly, two oblique layer unit cells and the layer displacement vectors $\vec{t}_1$ and $\vec{t}_2$ correspond to individual enantiomorphs and are related to each other by the pseudo-mirror plane (Figure 5), form the same defect-free *1Tc* kaolinite. A random interstratification of $\vec{t}_1$ and $\vec{t}_2$ vectors within individual kaolinite crystallites creates right-hand and left-hand kaolinite sequences thus producing structural disorder. A third layer displacement vector, $\vec{t}_0$, located along the long diagonal of the oblique layer unit cell that contains the vacant octahedral site and coincides with the layer pseudo-mirror plane may exist. This model attempts to estimate Pt_1, Pt_2 and Pt_0 which are the proportions (probability) of $\vec{t}_1$, $\vec{t}_2$, and $\vec{t}_0$ layer displacement translations, respectively within the structure.

The B-layers used in the simulation of the XRD pattern is as given by Bish and Von Dreele (1989). The original unit layer is first, using the appropriate matrices, orthogonalized along the stacking direction. This leads to α and β both equaling 90° while the γ remains unchanged (89.82°). The starting (prior to refinement) layer displacement

vectors used for the simulations were those determined by Bish and Von Dreele (1989) with slight modifications by Sakharov et al. (2016):

$$\vec{t}_1 = -0.3681\,\vec{a} - 0.0225\,\vec{b} + 7.1545\,\vec{n}$$

$$\vec{t}_2 = -0.3499\,\vec{a} + 0.3047\,\vec{b} + 7.1545\,\vec{n}$$

$$\vec{t}_0 = -0.3154\,\vec{a} - 0.3154\,\vec{b} + 7.1545\,\vec{n}$$

where $\vec{n}$ is a unit-cell vector along the *c** axis.

All the calculated XRD patterns are in the range 5-70°2θ, employing CuKα radiation.

3.7.3 Parameters used in simulation and refinement

A free format control file was first created detailing the calculation to be executed (Figure 10). This file contains instrumental and profile description parameters, structural data, information about the type of layers including, their stacking and transitions from each other, the type of calculation (simulation or refinement) and the experimental data. These parameters are briefly discussed in the preceding paragraphs.

The instrumental and profile parameter section of the control file takes care of the contribution of the diffractometer to the observed XRD patterns since observed (experimental) XRD patterns are dictated not only by the structures (crystallographic, microstructural or polycrystalline) of the specimens, but also by the configuration of the diffractometer (X-ray source and instrumental aberrations). This section contains information such as the wavelength of the X-rays, instrumental aberrations (zero, sycos and sysin) and profile parameters. The instrumental sycos and sysin aberrations account

for 2theta shifts that could arise from physical and/or geometrical problems. The three aberration parameters were assigned values of zero not refined.

Broadening due to instrument and size were treated by convoluting the calculated pattern with Thompson–Cox–Hasting (Thompson et al., 1987) pseudo-voigt (combination of Gaussian and Lorentzian) profile function. The Lorentzian and Gaussian full widths at half-maximum, H_L and H_G, respectively, were calculated for a LaB_6 standard reference material (SRM 660b) and were plotted against theta (degrees) from which the U, V, W and X components of the Gaussian and Lorentzian components of the peak profile were extrapolated using the formula:

$$H^2_G = U \tan^2\theta + V \tan\theta + W$$

$$H_L = X \tan\theta$$

The four components were fixed during refinement. Parameters for isotropic size broadening were also specified but the values were refined.

The structural information includes the cell parameters of the orthogonized unit cell ($a = 5.1554$ Å, $b = 8.9448$ Å, $c = 7.1557$ Å, $\alpha = \beta = 90°$ and $\gamma = 89.82°$), Laue symmetry (-1) and the width of the layer. Cell parameters a, b, c and γ were all refined.

In the layer section, the number of layers, the layer symmetry, atoms in each layer and their respective coordinates were specified. For the model to be adopted, all the layers were equal but different in translation vectors. The coordinates of the atoms are slightly different from the original unit cell prior to orthogonization of the unit cell.

The stacking type was specified as a recursive sequence of layers. “Recursive” indicates that the diffracted intensities are calculated for the statistical ensemble of crystallites, each

with a distinct stacking sequence, but weighted by the probability of existence of such sequence. For any given sequence, the wave function from any layer is equal to the sum of the wavefunction from that layer and the wavefunction of the displaced layer.

The transition section contained the translation vectors (relative to x, y and z) of one layer to another and the probabilities of occurrence of such layers.

3.8 Influence of Structural Disorder on Kaolinite Properties

To address the third objective, a thermal stability experiment was conducted to investigate if structural disorder affects basic properties of the mineral.

3.8.1 Thermal Stability

This experiment was conducted on a XRK 900 heating chamber. This chamber allows for *in-situ* XRD investigations while samples are heated. The three kaolinite samples were heated at 30, 400, 425, 450, 475, 500, 525 and 550 ºC while the XRD pattern were collected at each temperature. The rate at which the kaolinite mineral in the samples is destroyed, as measured by the rate of disappearance of the *001* diffraction peak, is used as a measure of the thermal stability of the mineral. A correlation is then investigated between the abundance of stacking disordering in kaolinite and thermal stability.

```
97t1_3t2 - Notepad
File  Edit  Format  View  Help
TITLE
97t1 and 03t2

 INSTRUMENTAL AND SIZE BROADENING
!Type Of Radiation
 Radiation          X-Ray
!                  lambda1     lambda2    ratio
 Wavelength         1.5406     1.5444     0.5
!instrumental aberrations          zero       sycos      sysin
 Aberrations                     0.00000    0.00000    0.00000
                                  0.00       0.00       0.00
!instr. broadening       u           v           w           x          Dg          Dl
 Pseudo-Voigt           0.0013    -0.0005     0.0001      0.0333    900000      400
                         0.00       0.00        0.00        0.00      0.00       99.00
 STRUCTURAL
   SPGR     P 1
 !          a           b           c          alpha    beta      gamma
 Avercell  5.1554      8.9448      7.40480     91.7    104.862   89.822
   !         a           b           c
 Cell      5.156110    8.944800    7.1557    89.82
           0.00        0.00        0.00      0.00

! FullProf Studio commands
FST_CMD  SEQ 11 1 1 2 1 3 2 2 3 3 1 1
FST_CMD  stack_vect  0 0 1.0
FST_CMD  box  0.0 1.0  0.0 1.0  0.0 1.0

!Laue symmetry
 Symm      -1
!number of layer types
 Nlayers  2
!layer width
 Lwidth   infinite

  LAYER 1
!Layer symmetry
 LSYM   none
!Atom name    number    x          y          z          Biso       Occ
 Atom Al3+         1    0.1232     0.4844     0.4721     0.0105     1
                        0.00       0.00       0.00       0.00       0.00
!Atom name    number    x          y          z          Biso       Occ
 Atom Al3+         2    0.6195     0.3188     0.4697     0.0105     1
                        0.00       0.00       0.00       0.00       0.00
!Atom name    number    x          y          z          Biso       Occ
 Atom Al3+         3    0.6232     0.9844     0.4721     0.0105     1
                        0.00       0.00       0.00       0.00       0.00
!Atom name    number    x          y          z          Biso       Occ
 Atom Al3+         4    0.1195     0.8188     0.4699     0.0105     1
                        0.00       0.00       0.00       0.00       0.00
!Atom name    number    x          y          z          Biso       Occ
 :         :         :          :          :          :          :

 Atom H           31    0.76307    0.48813    0.73920    1.0000       1
                        0.00       0.00       0.00       0.00       0.00
!Atom name    number    x          y          z          Biso       Occ
 Atom H           32    0.26307   0.98813     0.73920    1.0000       1
                        0.00       0.00       0.00       0.00       0.00
!Atom name    number    x          y          z          Biso       Occ
 Atom H           33    0.78423    0.79988    0.73740    1.0000       1
                        0.00       0.00       0.00       0.00       0.00
!Atom name    number    x          y          z          Biso       Occ
 Atom H           34    0.28423    0.29988    0.73740    1.0000       1
                        0.00       0.00       0.00       0.00       0.00

LAYER 2 = 1

 STACKING
!stacking type
 Recursive
!number of layers
infinite
 TRANSITIONS

!layer  1 to layer  1
LT      0.97000    -0.368900   -0.02230      1.000000
        0.00         0.00        0.00         0.00
FW      0.000000    0.000000    0.000000     0.000000     0.000000     0.000000
          0.00        0.00        0.00         0.00         0.00         0.00

!layer  1 to layer  2
LT      0.030000   -0.34880     0.305100     1.000000
        0.00        0.00        0.00         0.00
FW      0.000000    0.000000    0.000000     0.000000     0.000000     0.000000
          0.00        0.00        0.00         0.00         0.00         0.00


!layer  2 to layer  1
LT      0.030000   -0.34880     0.305100     1.000000
        0.00        0.00        0.00         0.00
FW      0.000000    0.000000    0.000000     0.000000     0.000000     0.000000
          0.00        0.00        0.00         0.00         0.00         0.00

!layer  2 to layer  2
LT      0.970000   -0.368900   -0.02230      1.000000
        0.00        0.00        0.00         0.00
FW      0.000000    0.000000    0.000000     0.000000     0.000000     0.000000
          0.00        0.00        0.00         0.00         0.00         0.00

 CALCULATION
 LMA
 Corrmax      30
 Maxfun     2400
 Tol      0.100000E-04
 Nprint       0

 EXPERIMENTAL
!Filename                    Scale factor      code
 File  Kaolinite.dat            1             12.00
 Fformat   FREE
!Linear interpolation
 BgrInter     BgTopasFdsPt2.bgr
```

Figure 10. An example of free a format control for the refinement of a kaolinite XRD pattern assuming 97 and 3% t_1 and t_2 translation vectors, respectively.

4. RESULTS AND DISCUSSION

4.1 Electron Microscopy

4.1.1 Scanning electron microscopy

Going by the SEM micrographs and corresponding EDS patterns of KGa (Figures 11 to 14), the sample contains primarily coarse kaolinite particles occurring as elongated, large vermiform stacks. This morphology is characteristic of specimens with low degree of structural disorder. The EDS of the kaolinite particles also reveals that the crystals are pure with no trace of any other elements within the structure. Accessory minerals in the sample include, zircon, muscovite and titanium oxide which is anatase since it has a non-prismatic morphology.

The SEM micrographs of WAI (Fig. 15 to 17) reveals that unlike the geologic sample, the soil sample contained smaller size and irregularly shaped particles. There were no distinct separated kaolinite crystals; instead the particles were intricately associated with each other or coatings. The observable kaolinite particle (Fig. 15) had a round shape with no evidence of stacking. This is evidence that the kaolinite in the WAI sample has a high degree of structural disorder. Accessory minerals identified in the SEM include mica, titanium oxide, iron oxide and ilmenite.

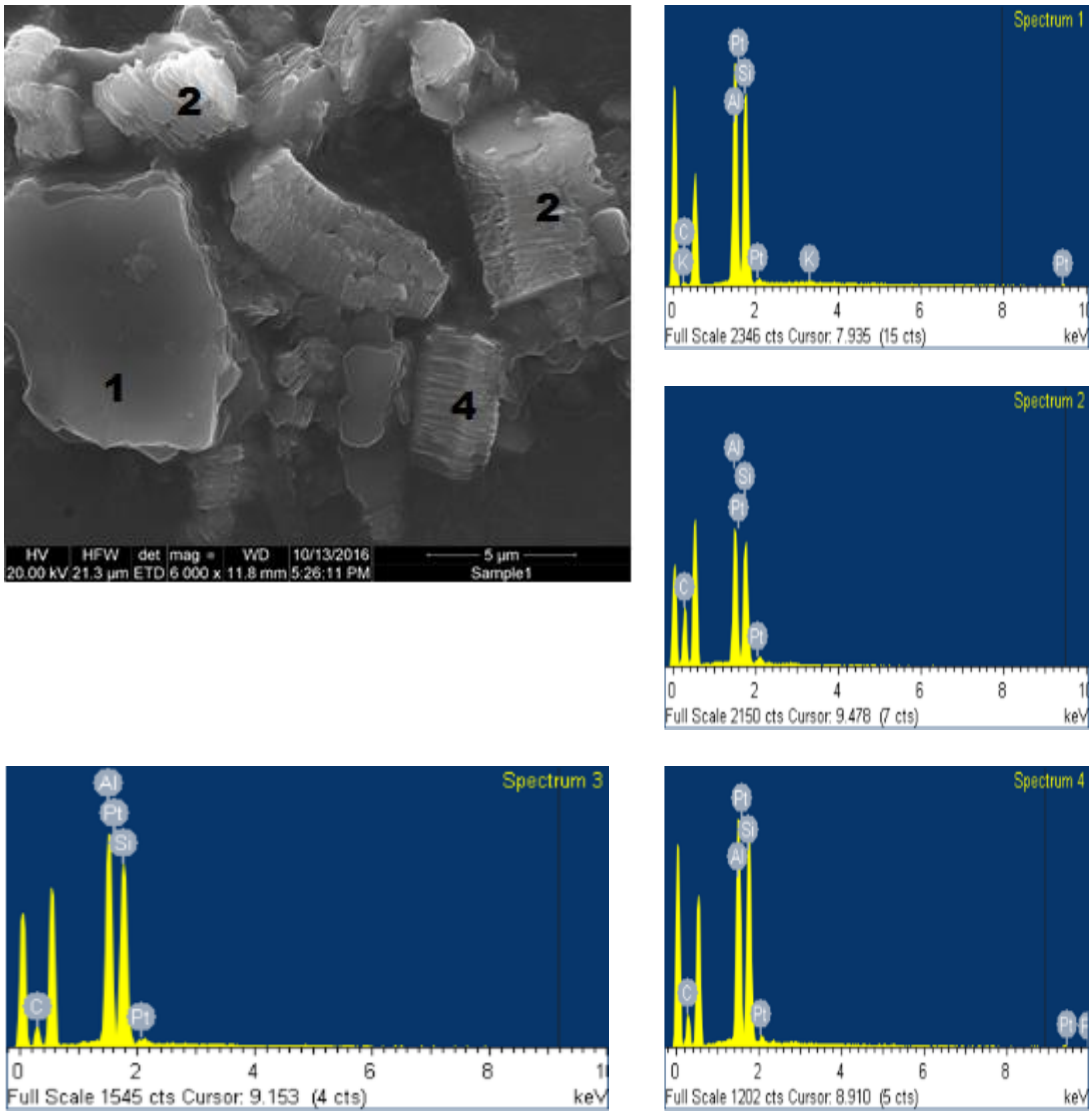

Figure 11 SEM micrograph and EDS pattern of kaolinite in silt fraction of KGa at 6000x magnification

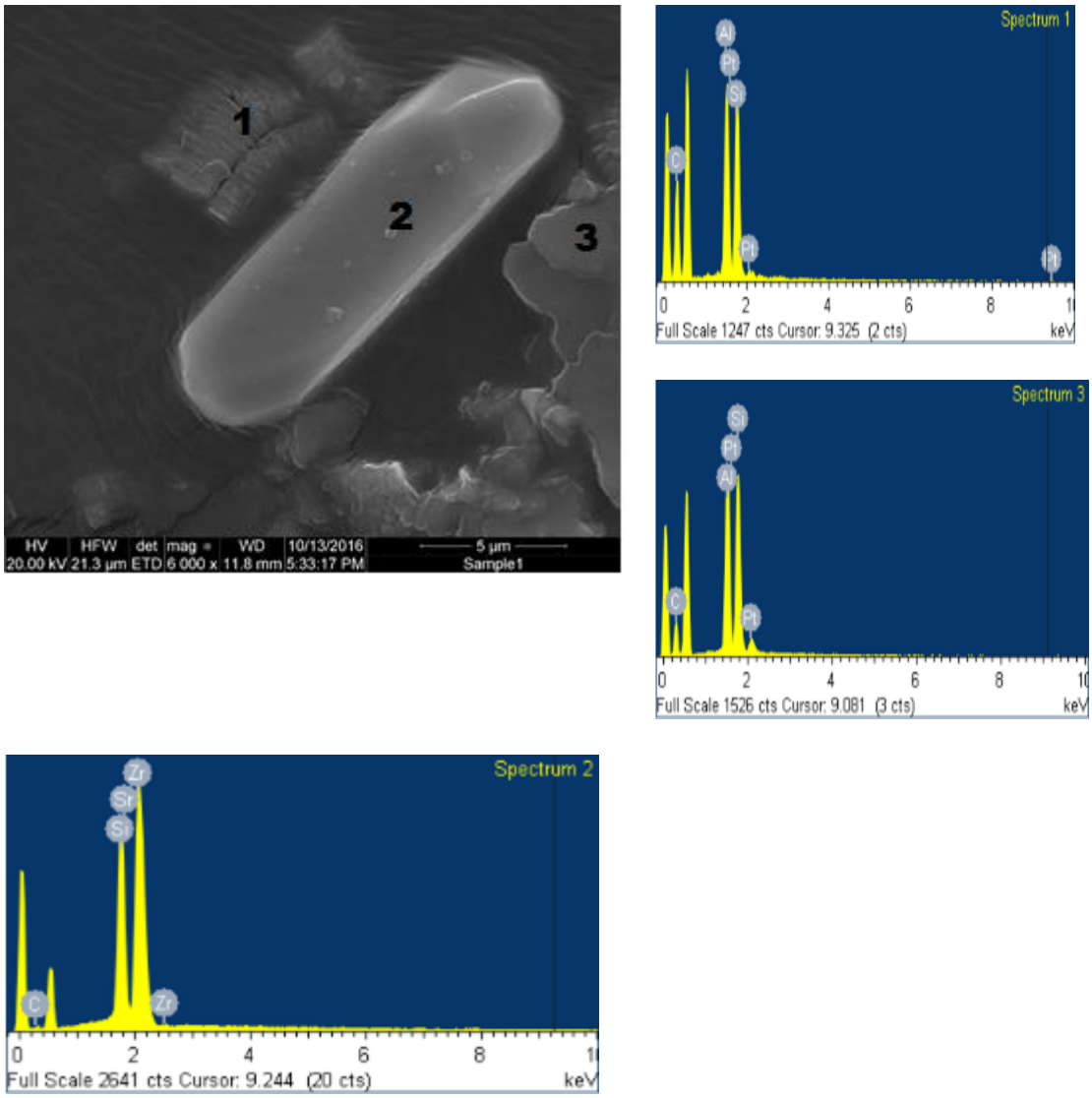

Figure 12 SEM micrographs and EDS pattern of kaolinite (spot 1 and 2) and zircon (spot 3) in silt fraction of KGa at 6000x magnification

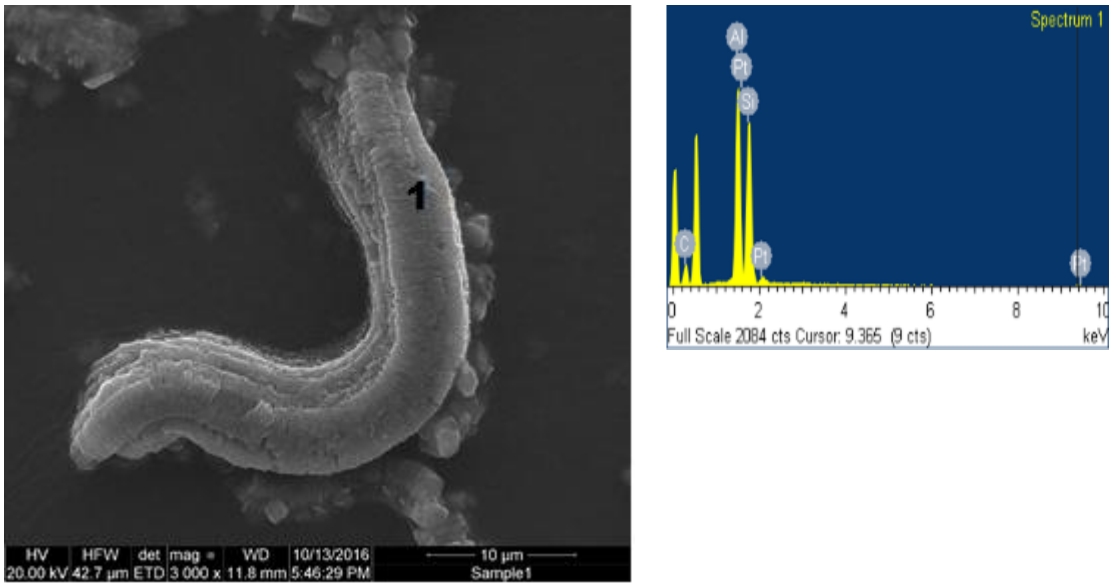

Figure 13 SEM image and EDS pattern of kaolinite in KGa at 3000x magnification

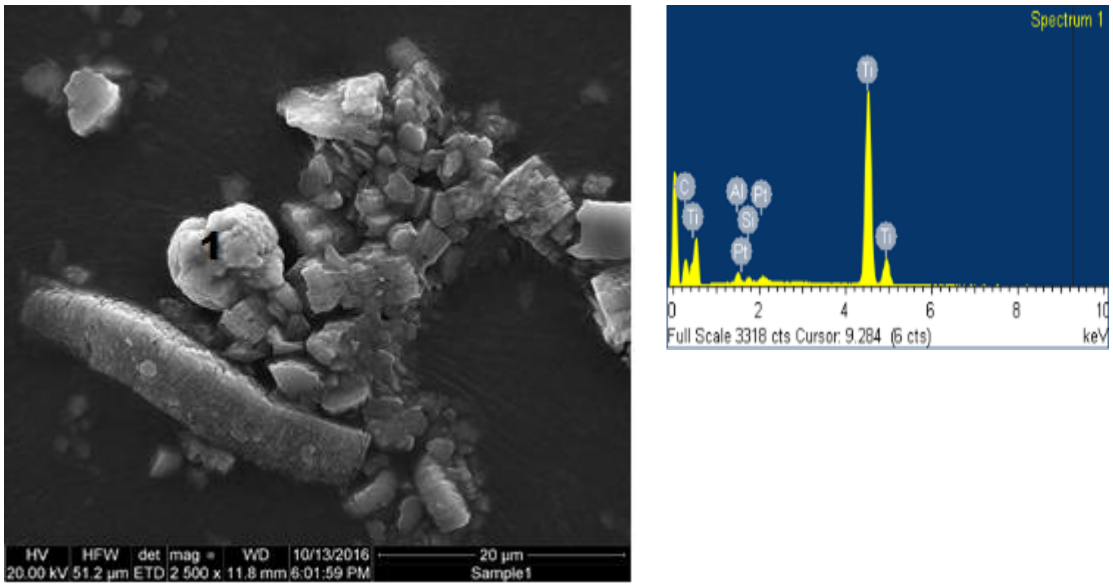

Figure 14 SEM of micrographs and EDS pattern of anatase in silt fraction of KGa at 2500x magnification

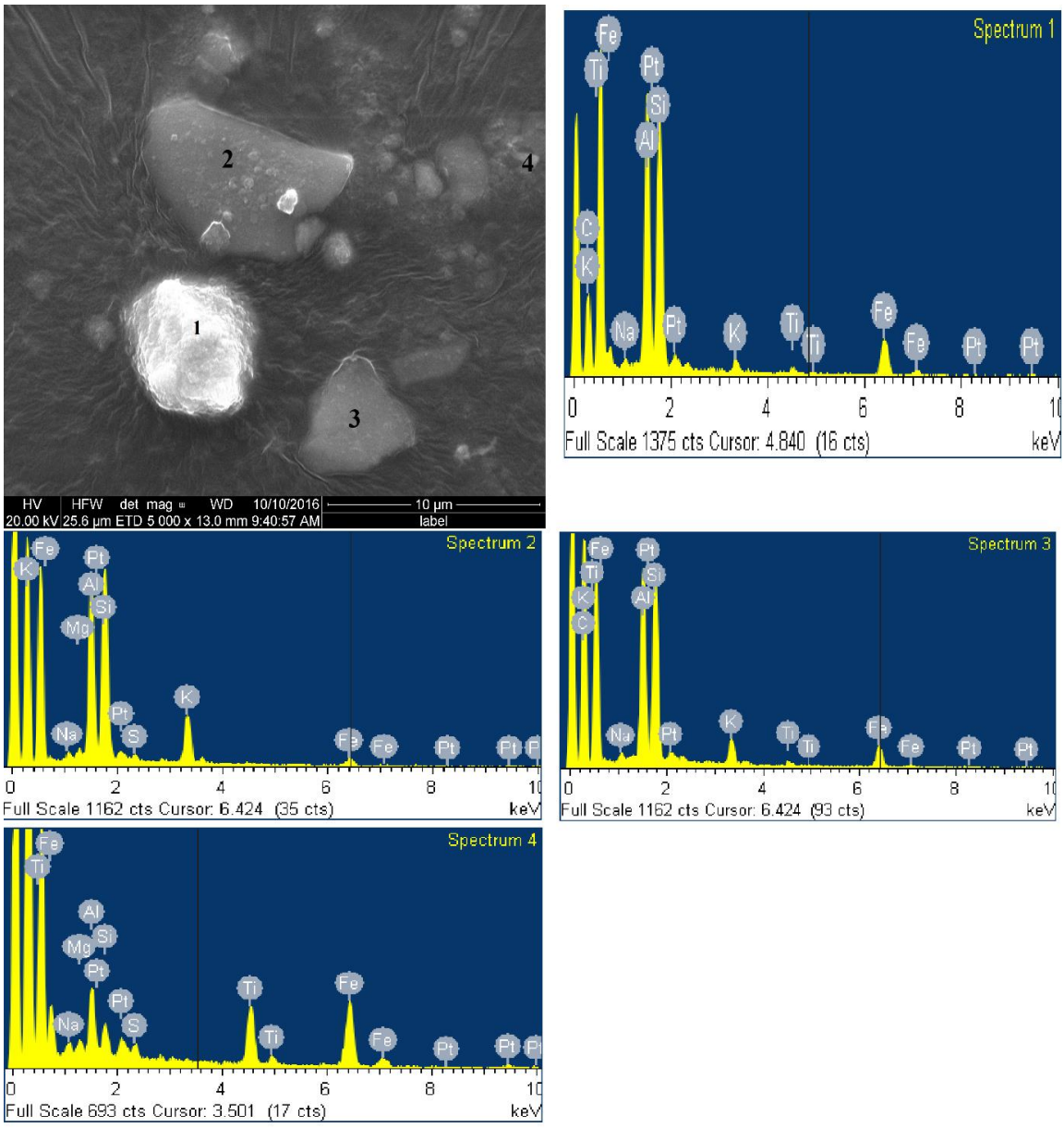

Figure 15 SEM micrographs and EDS pattern of kaolinite with iron oxide coatings (spot 1), mica and gibbsite particles (spot 2 and 3) and ilmenite and gibbsite particles (spot 4) in silt fraction of WAI at 5000x magnification

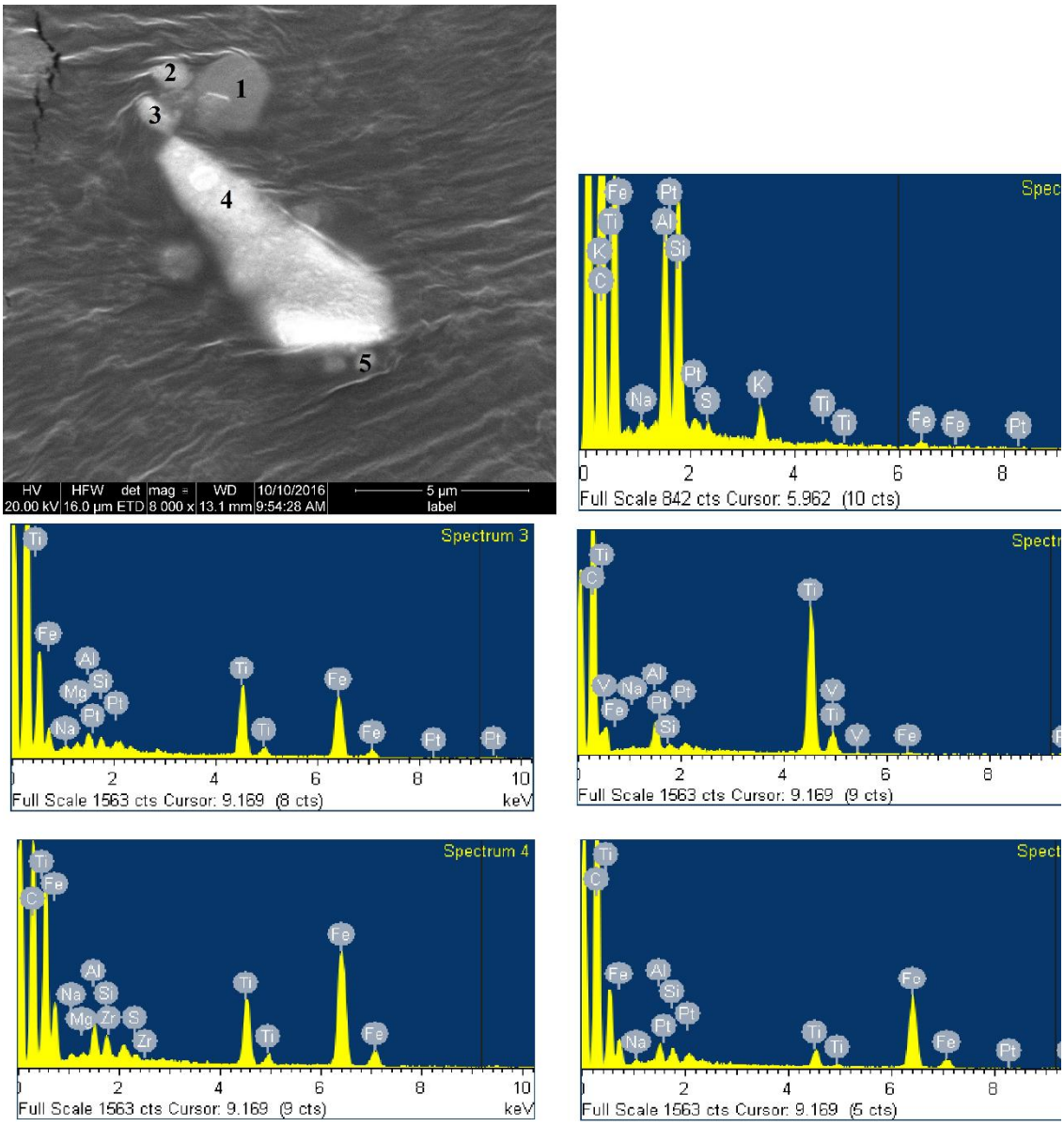

Figure 16 SEM micrographs and EDS pattern of mica and gibbsite particles (spot 1), titanium oxide (spot 2), ilmenite and gibbsite particles (spot 3 and 4) and iron oxide (spot 5) in silt fraction of WAI at 8000x magnification

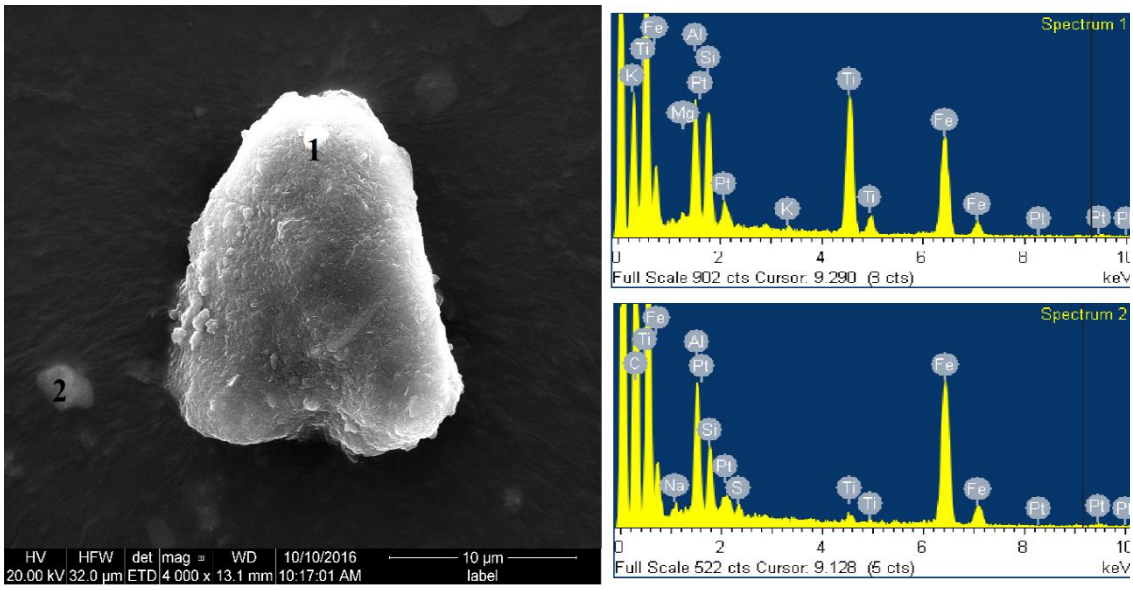

Figure 17 SEM micrograph and EDS pattern of an aggregate of kaolinite, ilmenite and iron oxide in silt fraction of WAI at 4000x magnification

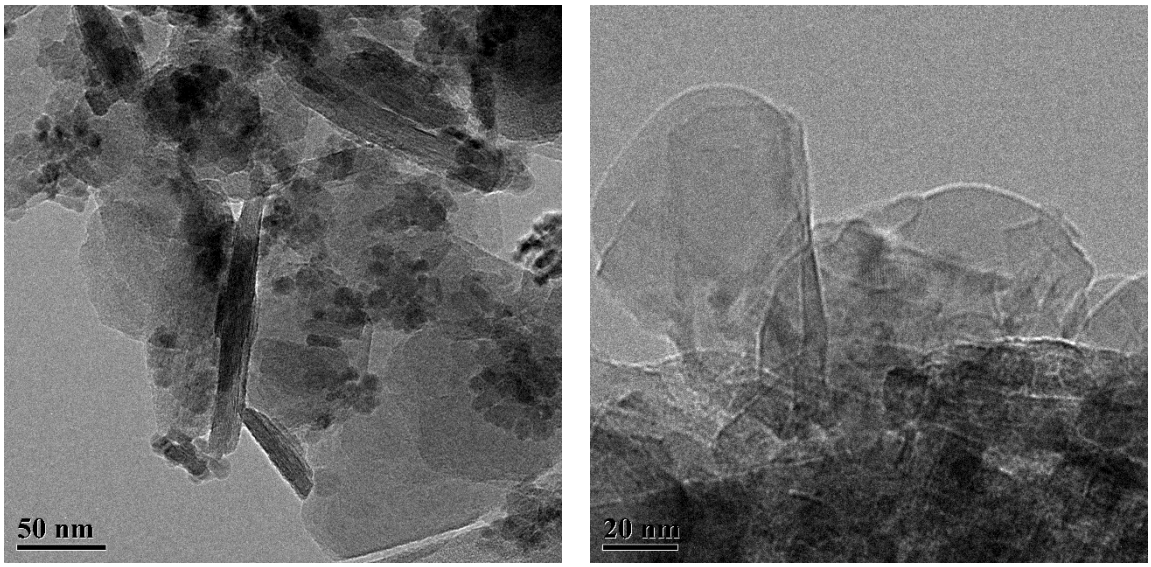

Figure 18 TEM micrographs of kaolinite in the clay fraction of WAI showing several showing several morphology and sizes

4.1.2 Transmission electron microscopy

The TEM micrographs of the clay fractions of WAI and BRZ are as shown in Figure 18. The observed kaolinite particles were very fine and exhibited several morphologies such as round, platy and tubular.

4.2 Instrumental Resolution Parameter

The XRD pattern for LaB_6, the Gaussian and Lorentzian plots are as shown in Figs. 19, 20a and 20b, respectively. The values of U, V, W and X were 0.0013, -0.0005, 0.0001 and 0.033, respectively. These values were inputted in FAULTS to describe broadening that may occur due to instrumental configuration.

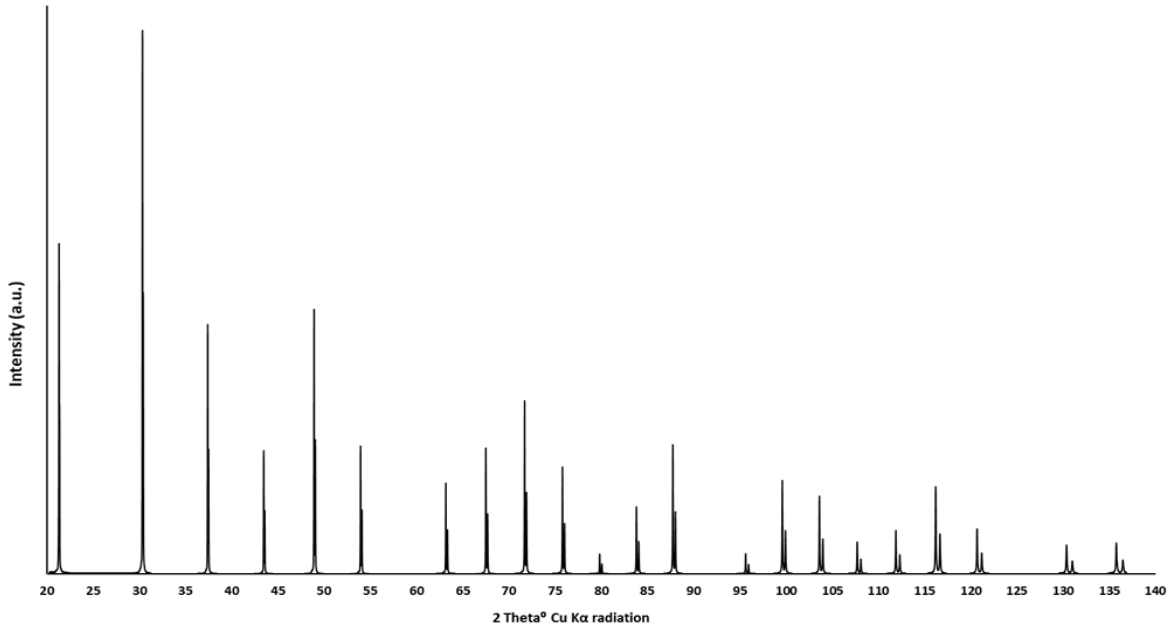

Figure 19 X-ray diffraction pattern of LaB_6

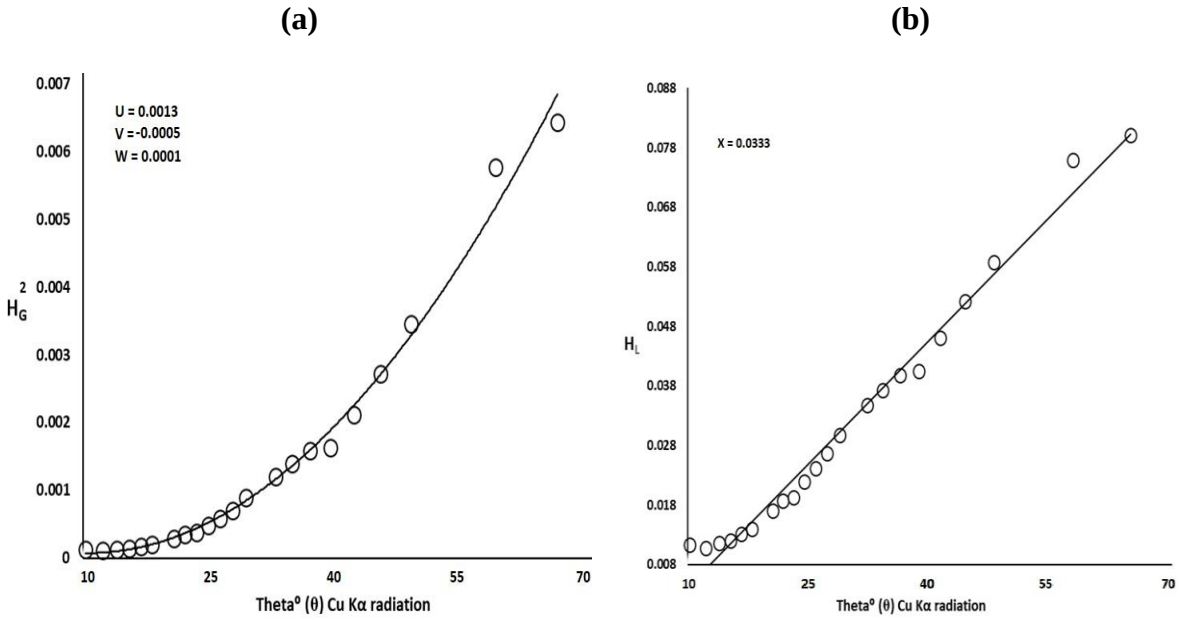

Figure 20. The (a) Gaussian and (b) Lorentzian plots from the LaB_6 XRD pattern

4.3 Experimental XRD Patterns

The XRD patterns of the unsprayed KGa (black) and the spray-dried version (red) are shown in Fig. 21. The primary difference between the two patterns is in the intensity of the *001* and *002* reflections which were 20 and 12%, respectively more intense in the unsprayed sample. Under a microscope, the morphology of the spray-dried sample was primarily constituted by spherical aggregates (Fig. 22). Consequently, the spray-dried pattern was used as the experimental XRD pattern prior to simulation and refinement. Accessory minerals in the KGa sample are mica, quartz and anatase. The KGa is a weakly disordered kaolinite as evident in the high resolution and separation of the four reflections between 19.83°2θ and 23.44°2θ. A strange feature of this sample is a significant

background between 19.83°2θ and 23.44°2θ. The co-existence of highly resolved peaks between 19.83°2θ and 23.44°2θ and the high background between 19.83°2θ and 23.44°2θ in one sample is a *coincidentia oppositorum* since the latter is characteristic of moderate to highly disorder kaolinite while the former is a feature of weakly disordered kaolinite.

The dominant mineral in the clay fraction of BRZ is kaolinite while accessory minerals are gibbsite, quartz, anatase, rutile and vermiculite (Fig. 23). The high background and the disappearance of some kaolinite reflections between 19.83°2θ and 23.44°2θ are indications that the BRZ is a highly disordered sample. Also, other kaolinite reflections at higher angles are either missing or poorly resolved.

The dominant mineral in WAI is gibbsite followed by kaolinite. Other minerals in the sample are anatase, mica, rutile, ilmenite, quartz and hematite (Fig. 24).

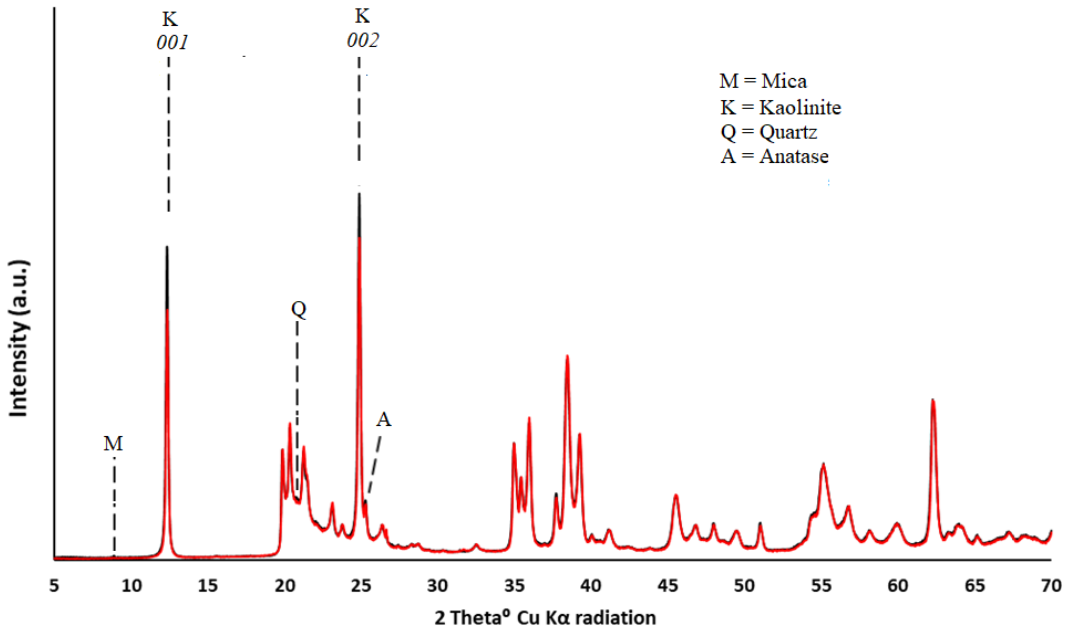

Figure 21. Experimental XRD patterns of unsprayed (black) and spray-dried (red) KGa

(a)

(b)

Figure 22 Morphology of (a) sprayed-dried and (b) unsprayed KGa as viewed at X6 under a light microscope

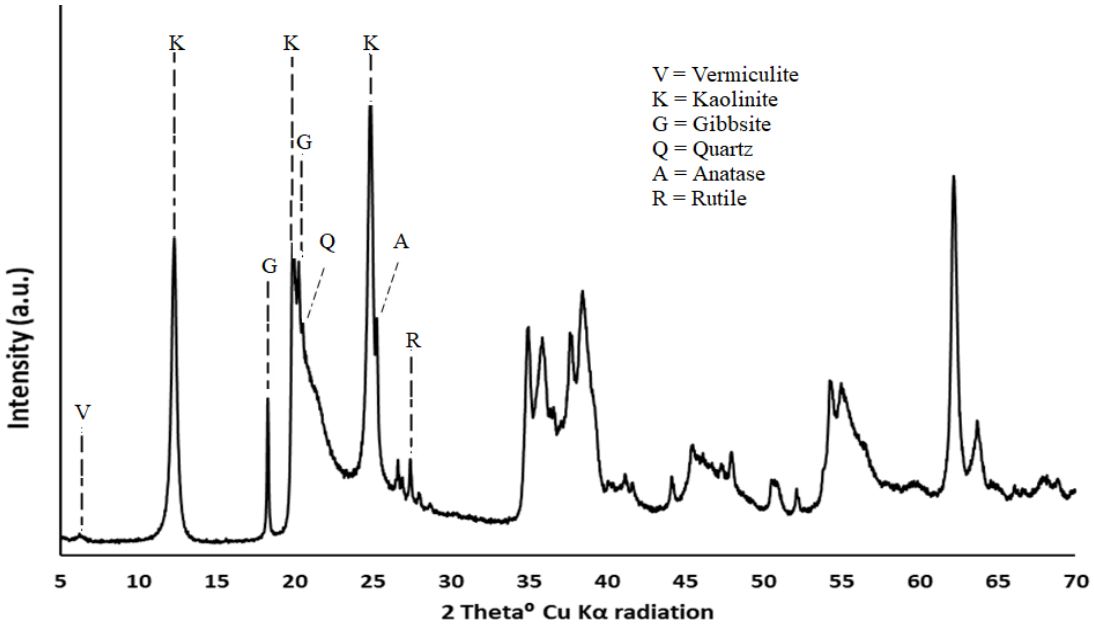

Figure 23 Experimental XRD pattern of BRZ

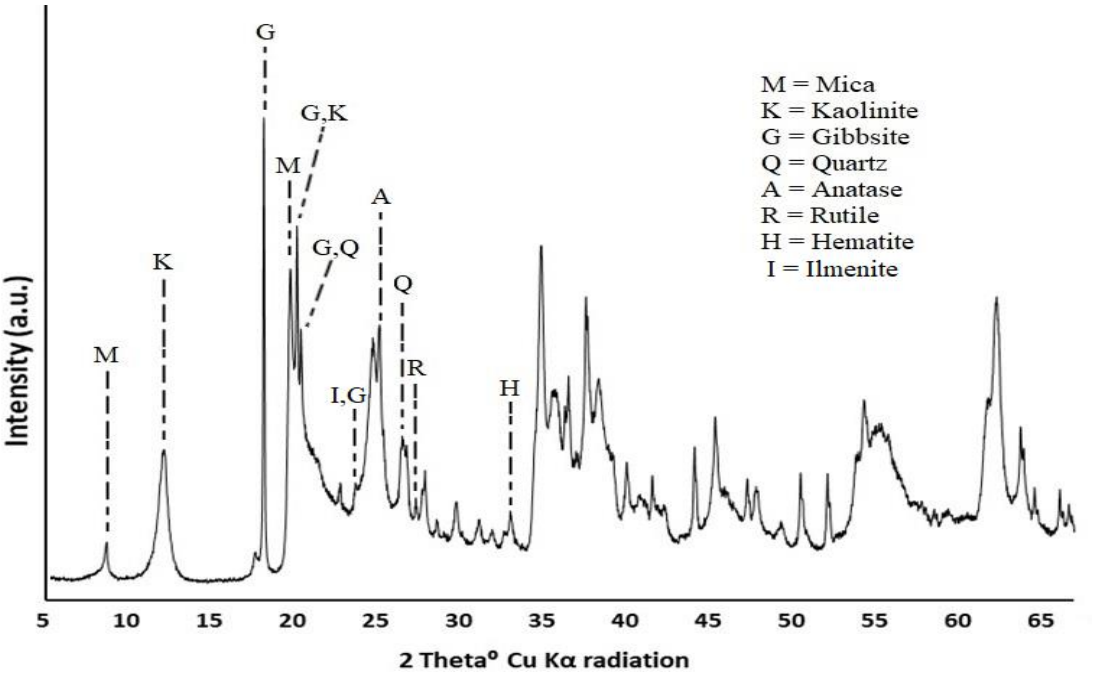

Figure 24. Experimental XRD pattern of WAI

4.4 Minimizing Interferences by Accessory Minerals

4.4.1 Thermal destruction of accessory minerals

The XRD pattern of the sample at room temperature (R), 300 °C (T), and at 550 °C (F) are as shown in Fig. 25. The diffraction peaks corresponding to gibbsite disappeared after the 330 °C leaving behind the diffraction peaks of kaolinite and the other accessory minerals such as mica, quartz, etc. At 550 °C the peaks corresponding to kaolinite have all disappeared indicating a complete dehydroxylation of the mineral. At this point the XRD pattern only contained the accessory minerals.

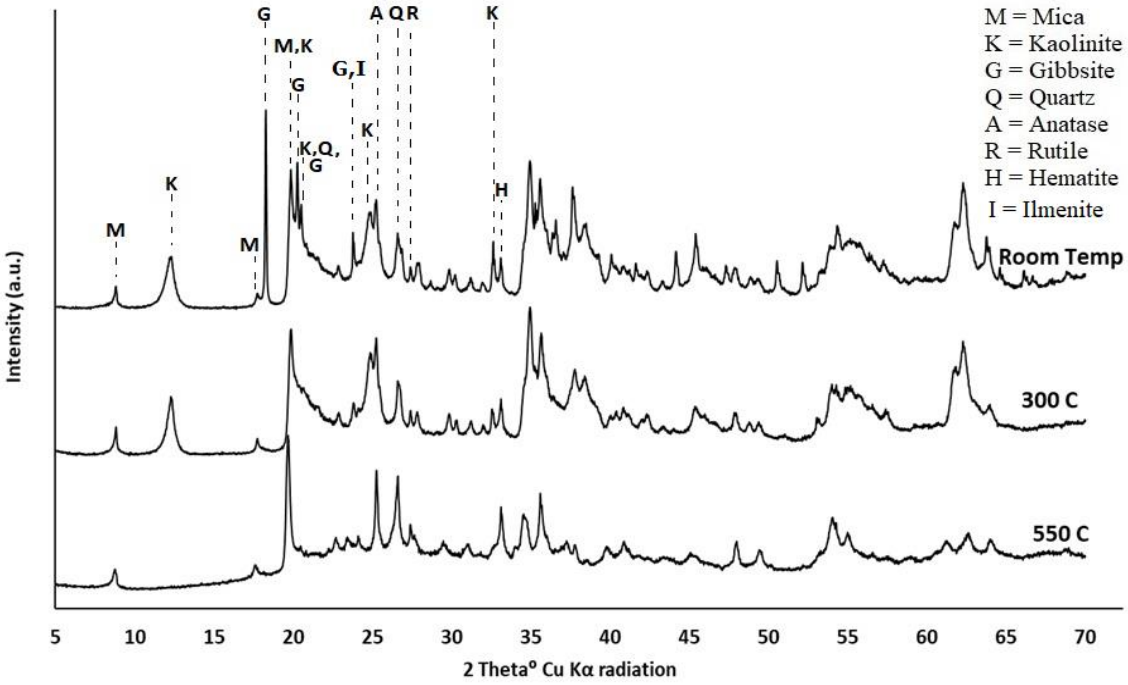

Figure 25 XRD patterns of WAI at room temperature, 300 and 550 °C

The XRD pattern determined by subtraction, as explained in section 3.6.1, are as shown in Fig. 26. Attempt to achieve a pure kaolinite pattern was not successful as shown by the kaolinite pattern in Fig. 26. The probable reason for this is that the sequential thermal destruction left behind amorphous phases of the mineral destroyed. For example, the thermal destruction of gibbsite at 300 °C will result in an amorphous phase of the mineral and this also applies to the destruction of kaolinite at 500 °C. Thus, the pattern titled "Kaolinite + Accessory minerals" which is supposed to be pattern representing just kaolinite, other accessory minerals but without gibbsite contains kaolinite, accessory minerals and amorphous phases (including amorphous gibbsite). Since the subtractions could not account for the amorphous phases of gibbsite and kaolinite, the final pattern "Kaolinite" had diffraction peaks with negative intensities. Another reason for the lack of success using this method was the shifting of certain diffraction peaks after the heating experiment. For example, the mica peaks shifted asymmetrically in the 500 °C pattern compared to the room temperature pattern. Hence subtraction lead to some diffraction peaks having negative intensities. Yet this approach was important in revealing that mica was the major contributor to the diffraction peak at about 20°(2θ) since the pattern at 500 °C has the peak still as intense as it was in the room temperature pattern.

In view of the failure to mathematically arrive at a relatively pure kaolinite pattern using the thermal destruction approach due to inability to account for amorphous phases of the destroyed minerals and the asymmetric shifting of certain diffraction peaks, the Rietveld approach was evaluated.

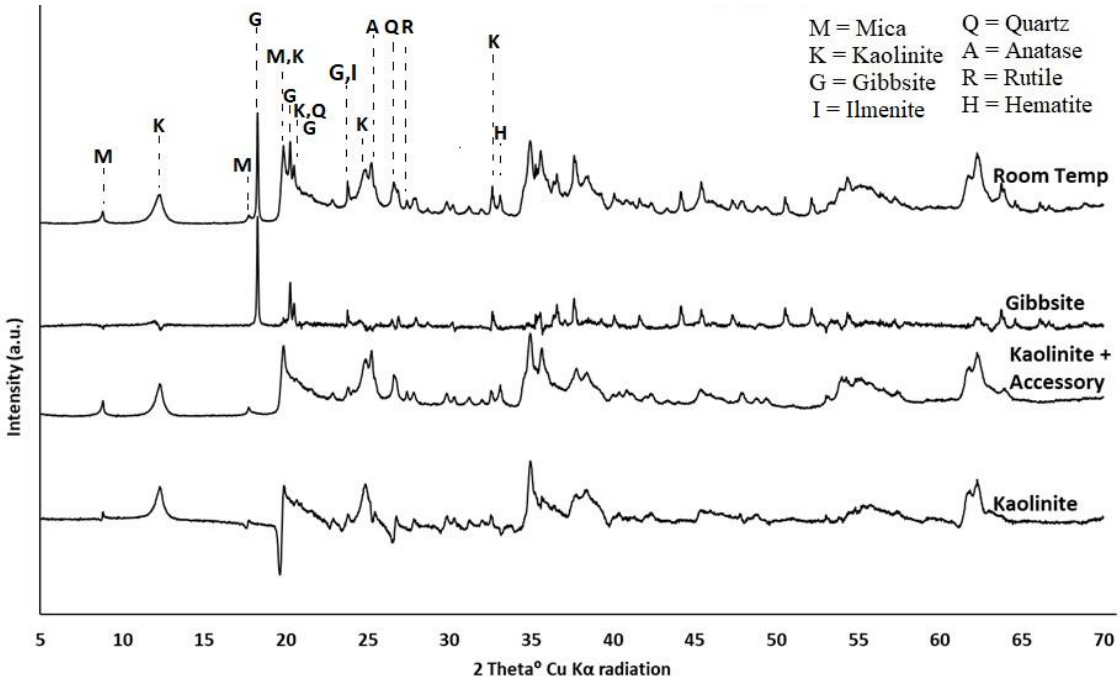

Figure 26. XRD patterns of different mineral phase in WAI after subtractions

4.4.2 Rietveld approach

The quantification of phases in the BRZ and WAI sample is shown in Fig. 27 and 28, respectively. The contribution of each accessory mineral to the experimental patterns of BRZ and WAI are as shown in Fig. 28 and 30, respectively.

The R_{wp} value after refinement for the BRZ sample was 10.62%. The most significant error in the calculated pattern after refinement is for the diffraction peak at about 20°2θ (*020* of kaolinite) which the calculated pattern could not sufficiently model. Also, the diffraction peaks at about 20 and 21°2θ belonging to gibbsite and kaolinite, respectively, were both excessively modeled. These three errors lead to the final kaolinite

pattern (Fig. 28) having strong diffraction peaks between 20 and 25°2θ. Such features are characteristic of kaolinite specimens with low degree of structural disorder which are not likely to be found in pedogenic kaolinites. For this reason, the final kaolinite pattern after refinement was not used as the experimental pattern during the study of disorder. Instead, prior to simulation and refinement of disordering, the XRD patterns of the accessory minerals that were calculated by Rietveld refinement were incorporated into FAULTS as background files.

The R_{wp} value after refinement for the WAI sample was 7.79% (Fig. 29). Again, there were errors in the calculated pattern like those in the BRZ sample. As in the case of the BRZ sample, the original experimental pattern was used for the study while the XRD patterns of the major accessory phases were used as background files.

Due to the high purity of the KGa sample, the little quantity of the accessory minerals is not expected to affect the modeling and refinement. Also, the accessory minerals contained in the sample does not share important diffraction peaks (in context to the study of structural disorder) with kaolinite.

Through the non-destructive Rietveld approach, it was possible to significantly quantify the contributions of the accessory minerals to the experimental patterns of BRZ and WAI. The XRD patterns of each accessory mineral is then used as background files in the FAUTS program. Through this, the influence of the accessory minerals on the overall diffraction peaks of the experimental XRD pattern was calculated and removed to improve the confidence in the structural model. By this, the problems associated with presence of accessory minerals is significantly reduced.

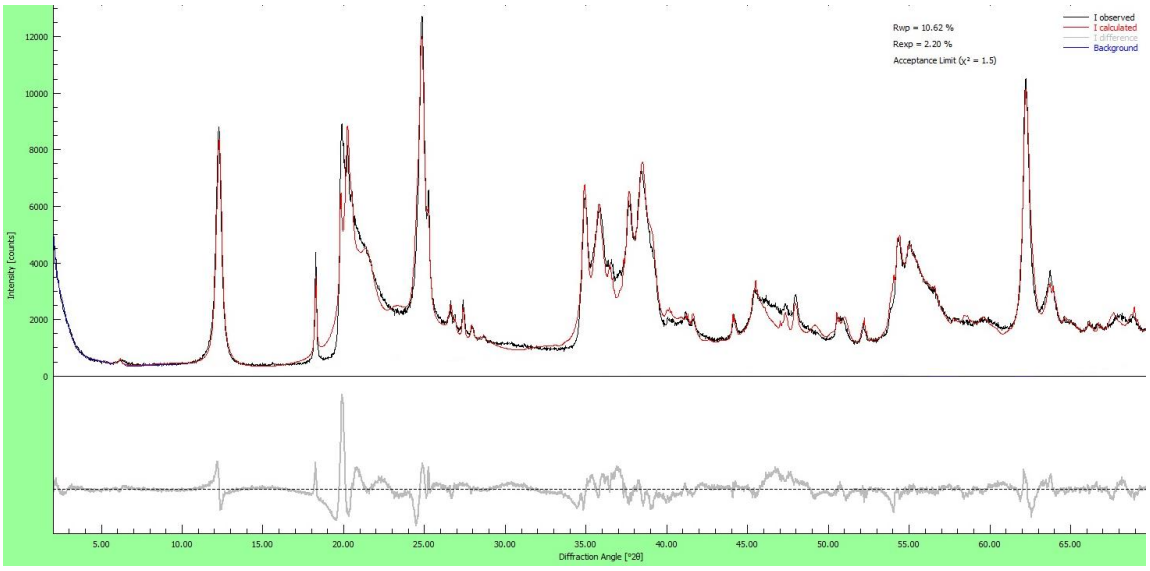

Figure 27. Quantification by Rietveld refinement for BRZ

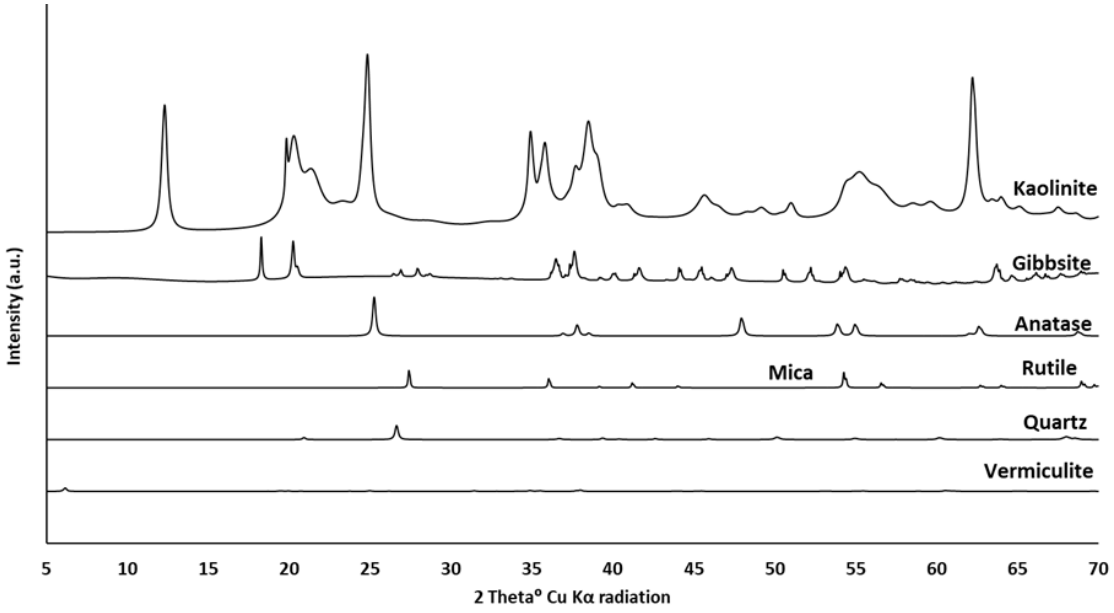

Figure 28. X-ray diffraction patterns, after background correction, corresponding to the accessory minerals in BRZ

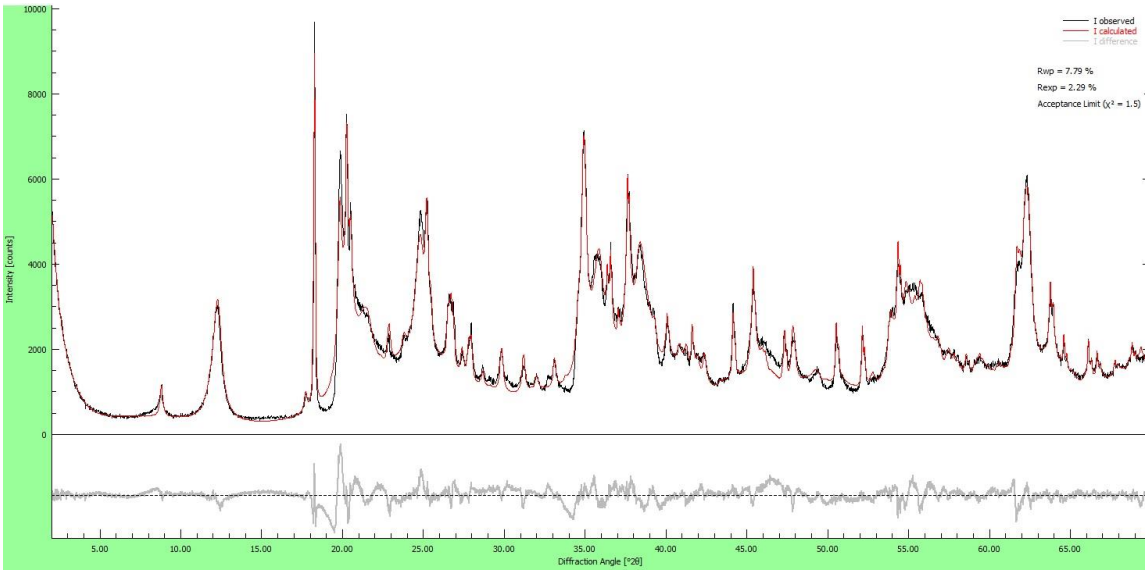

Figure 29. Quantification by Rietveld refinement for WAI

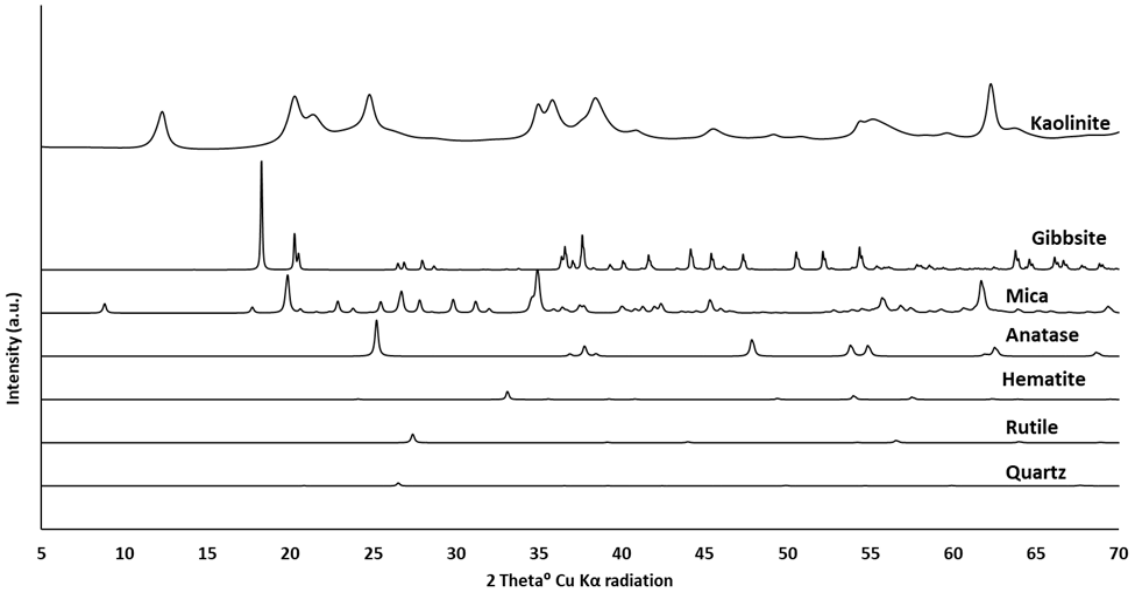

Figure 30. X-ray diffraction patterns, after background correction, corresponding to the accessory minerals in WAI

4.5 Simulation and Refinement of Calculated XRD Patterns

4.5.1 KGa

Attempts to simulate the KGa sample using a single-phase model by varying proportions of defects (by varying Pt_1, Pt_2, Pt_0 and Pt_a) could not reproduce the experimental XRD pattern of the sample. When high proportion of defects is introduced into the simulation the background between the 19.83°2θ and 23.44°2θ is indeed reproduced but the well separated peaks between 19.83°2θ and 23.44°2θ disappears (Fig. 31b). Also, the sharp peaks at higher angles become too smeared and incompatible with the experimental pattern. On the other hand, introduction of a low proportion of defects in the simulated XRD pattern reproduces the sharp and well separated peaks between 19.83°2θ and 23.44°2θ as well at the well the resolved peaks at higher angles characteristic of the KGa sample. But this simulated XRD pattern is yet incompatible with the experimental XRD pattern because of the inability to reproduce the background between 19.83°2θ and 23.44°2θ (Fig. 31a).

The inability to sufficiently reproduce the experimental XRD pattern stems from the co-existence of features of both low disordered kaolinite and a highly disordered kaolinite in a single sample. Plançon et al. (1988) made similar observation in a kaolinite sample and concluded that the simultaneous existence of sharp peaks (characteristic of low level of disorder) and a significant background between the peaks (characteristic of high level of disorder) could only mean that the sample consisted of two phases — one with almost no disorder and the other highly disordered. Earlier study by Deluca and

Slaughter (1985) using deconvolution technique to obtain XRD patterns also confirms the presence of multiple, well-crystallized kaolinite phases in a sample of Keokuk, Iowa geode-kaolinite.

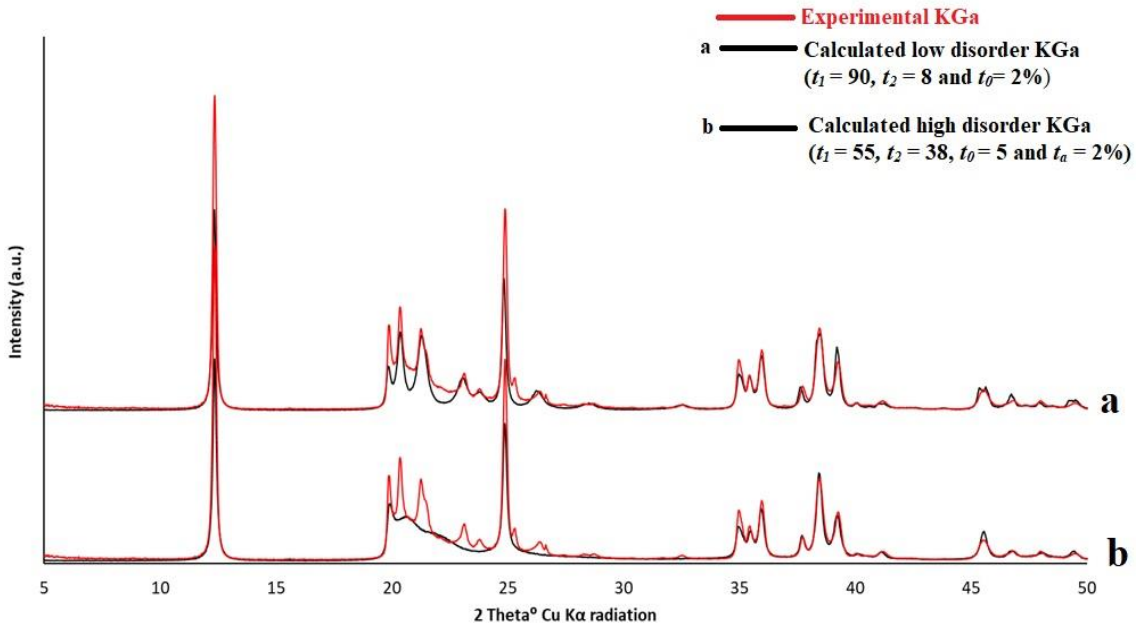

Figure 31. Simulated XRD patterns of a (a) low defect phase (Pt_1 = 90, Pt_2 = 8 and Pt_0= 2%) and (b) high defect phase (Pt_1 = 55, Pt_2 = 38, Pt_0 = 5 and Pt_a = 2%).

The possible co-existence of multiple kaolinite phases in the KGa sample was further investigated experimentally by acquiring XRD patterns of different size fractions of the sample (Fig. 32). For a single-phase kaolinite sample, it is expected that degree of

disordering will increase with decrease in particle size. Hence, the reflections between 19.83°2θ and 23.44°2θ are expected to become less sharp and poorly resolved as the

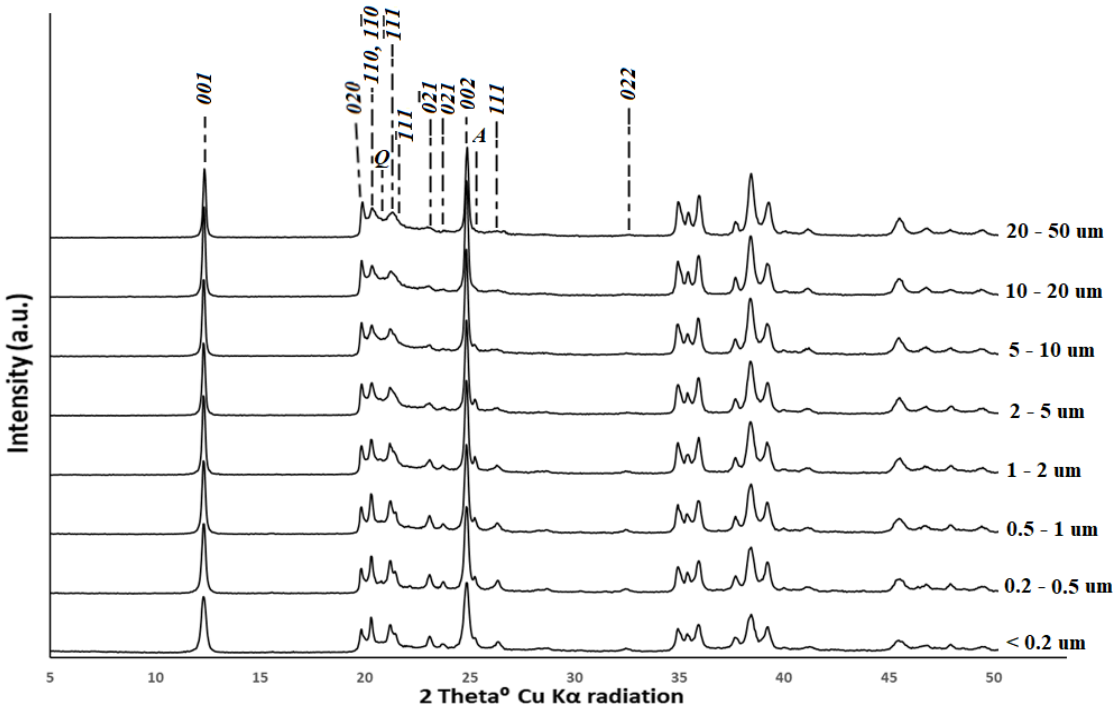

Figure 32. XRD patterns of different size fractions of in KGa

particle size decreases. Surprisingly, the XRD patterns of the different size fractions of KGa sample showed a decrease in structural disorder as the particle size decreased. The reflections *020, 110, -1-11, -111, 0-21* and *021* became more resolved and separated as the particle size decreased. The *-111* diffraction peak was too poorly resolved to be seen in the first four size fractions (20 – 50, 10 – 20, 5 – 10, and 2 – 5 µm) but very sharp and prominent in the last four fractions (1 – 2, 0.5 – 1, 0.2 – 0.5, and < 0.2 µm). Also, a

significant background exists in the first four fractions in comparison with the last four fractions. Using the *-111* reflection and the background as reference, the XRD patterns can be grouped into two phases — weakly disordered (1 – 2, 0.5 – 1, 0.2 – 0.5, and < 0.2 μm) and highly disordered (20 – 50, 10 – 20, 5 – 10, and 2 – 5 μm) phase. The Hinckley index (Hinckley, 1962) of the size fractions were also calculated to quantify the degree of disorder in each of the size fractions (Fig. 33). The figure shows that degree of structural disorder decreased with decrease in particle size. This is probably due to the high concentration of the weakly disordered phases in the smaller size fraction (1 – 2, 0.5 – 1, 0.2 – 0.5, and < 0.2 μm). More importantly, again, there seems to be two distinct HI groups — one with HI ranging 1.23 and 1.36 (almost no disorder phase) and the other with HI ranging from 0.81 and 1.00 (highly disordered phase). Going by the evidences gathered from the XRD patterns of the different particle size ranges of KGa, it is obvious that the sample is constituted by at least two phases. Hence , the two-phase approach suggested by Plançon et al. (1988) was used in the simulation of structural order in KGa.

The structural parameters used for the almost no disorder phase (NDP) was 97% of $\vec{t}_1$ layer displacements and 3% of $\vec{t}_2$ (enantimorphic fragments) while the highly disordered phase (HDP) was constituted by 55, 35, 5 and 5% of $\vec{t}_1$, $\vec{t}_2$, $\vec{t}_0$ and $\vec{t}_a$, respectively. Presently, the capability to simulate and refine disordering in two-phases of a single mineral has not been implemented in FAULT. To overcome this challenge, each phase (NDP and HDP) was individually simulated in FAULT while the proportion of each phase that best agrees with the experimental pattern was solved for in Excel. The XRD patterns corresponding to the NDP and HDP crystallite populations are as shown in Figure

34. Using the Solver add-on in Microsoft Excel, the best agreement between the experimental and calculated pattern was determined when taken in proportion 32.16% and 67.84%, of NDP and HDP, respectively, at Rp = 15% (Figure 35). The initial and final values of the unit cell parameters as well as the proportions of HDP and NDP in KGa are as shown in Table 2. Structural models of $\vec{t}_1$, $\vec{t}_2$ and $\vec{t}_0$ layers are shown in figure 36.

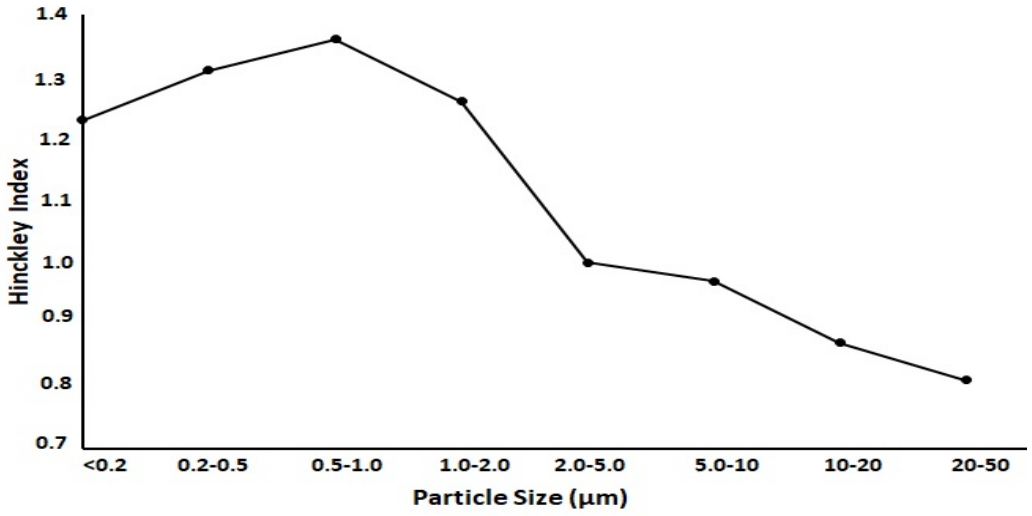

Figure 33. Graph of Hinckley index of KGa at different particle sizes

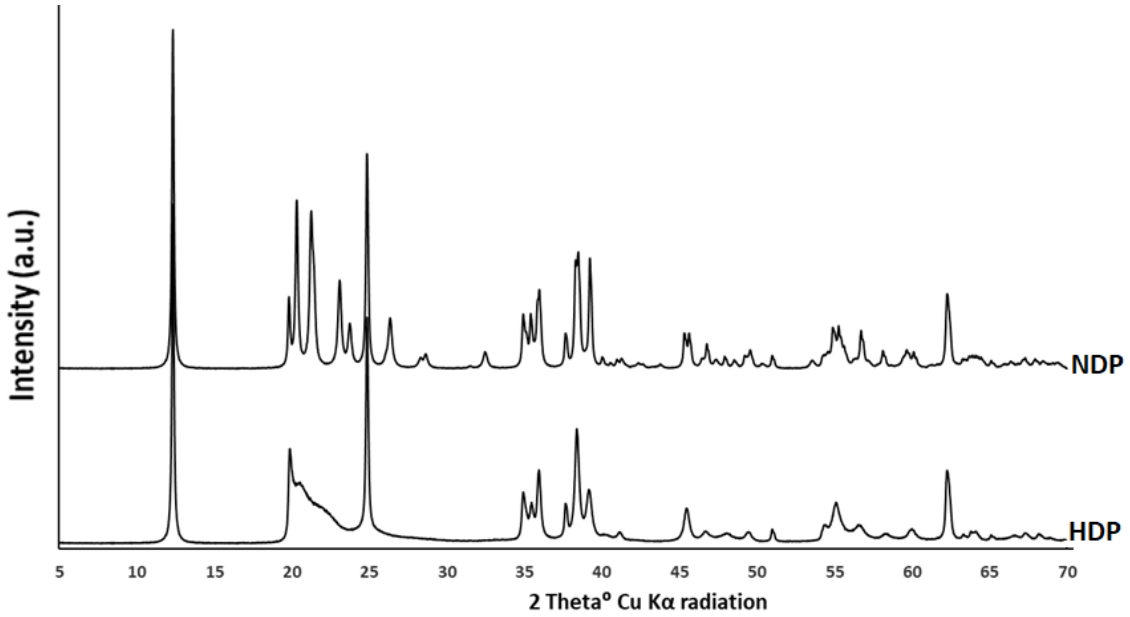

Figure 34. Simulated XRD patterns of the almost no disorder phase (NDP) and highly disordered phase (HDP).

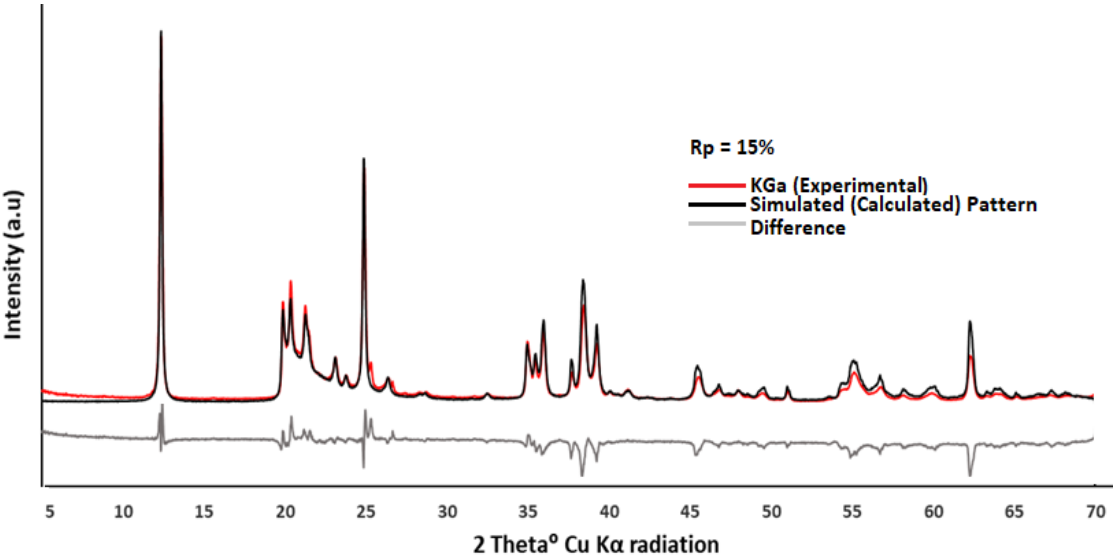

Figure 35. Experimental (red) and the calculated XRD (black) patterns of KGa

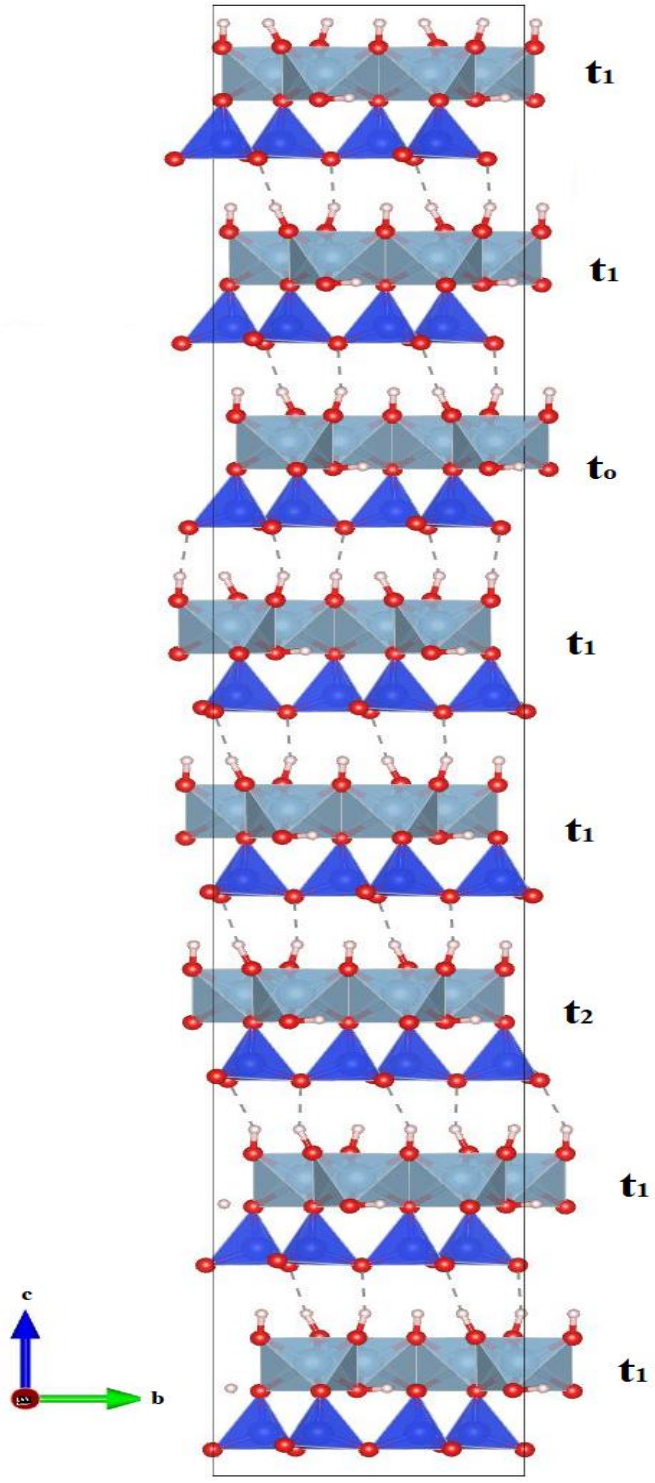

Figure 36 Structural models of a stack consisting of $\bar{t}_1$, $\bar{t}_2$ and $\bar{t}_0$ layers

Table 2. Structural parameters used in the simulation of NDP and HDP fractions in KGa.

Kaolinite Phases

	NDP	HDP
P (%)	32.16	67.84

Displacement Vectors

		$\vec{t}_1$	$\vec{t}_2$	$\vec{t}_0$
Initial		$-0.3681\,\vec{a} - 0.0225\,\vec{b}$	$-0.3499\,\vec{a} + 0.3047\,\vec{b}$	$-0.3154\,\vec{a} - 0.3154\,\vec{b}$
Final		$-0.3689\,\vec{a} - 0.0223\,\vec{b}$	$-0.3488\,\vec{a} + 0.3051\,\vec{b}$	$-0.3151\,\vec{a} - 0.3151\,\vec{b}$
P (%)	NDP	97	3	—
	HDP	55	35	5

Unit Cell Parameters

	a (Å)	b (Å)	c* (Å)	γ (deg)
Initial	5.1554	8.9448	7.1557	89.82
Final	5.1561	8.9448	7.1557	89.80

4.5.2 BRZ

As shown in Figure 23, in addition to kaolinite, the BRZ sample also contains vermiculite, gibbsite, anatase, rutile and some amorphous phases. These accessory minerals make simulation of structural disorder in the sample very tedious and render results unreliable. To overcome the challenge posed by the presence of additional minerals, there was need to quantify and block the reflections of the accessory minerals.

The quantification of other minerals was conducted using a Rietveld refinement program TOPAS (Bruker). Each accessory mineral was quantified in TOPAS while the patterns of each quantified phase was used as a background file in FAULTS. This is with the view to minimizing the influence of the accessory minerals and improving the agreement between the calculated and the experimental pattern. The best agreement between the experimental and calculated pattern was found when taken in proportion 45%, 35% and 20%, $\vec{t}_1$, $\vec{t}_2$, and $\vec{t}_0$, respectively, at Rp = 16.70% (Figure 37). The BRZ sample is highly disordered and contains a single phase in contrast to the KGa sample. The proportion of $\vec{t}_0$ calculated in the BRZ sample (20%) is higher than maximum limit (5%) calculated by Sakharov et al. (2016) for geologic kaolinites. This high value, $P\vec{t}_0$ = 20%, was necessary in reproducing the smearing of certain reflections at the higher angles. The initial and final values of the unit cell parameters for BRZ are as shown in Table 3.

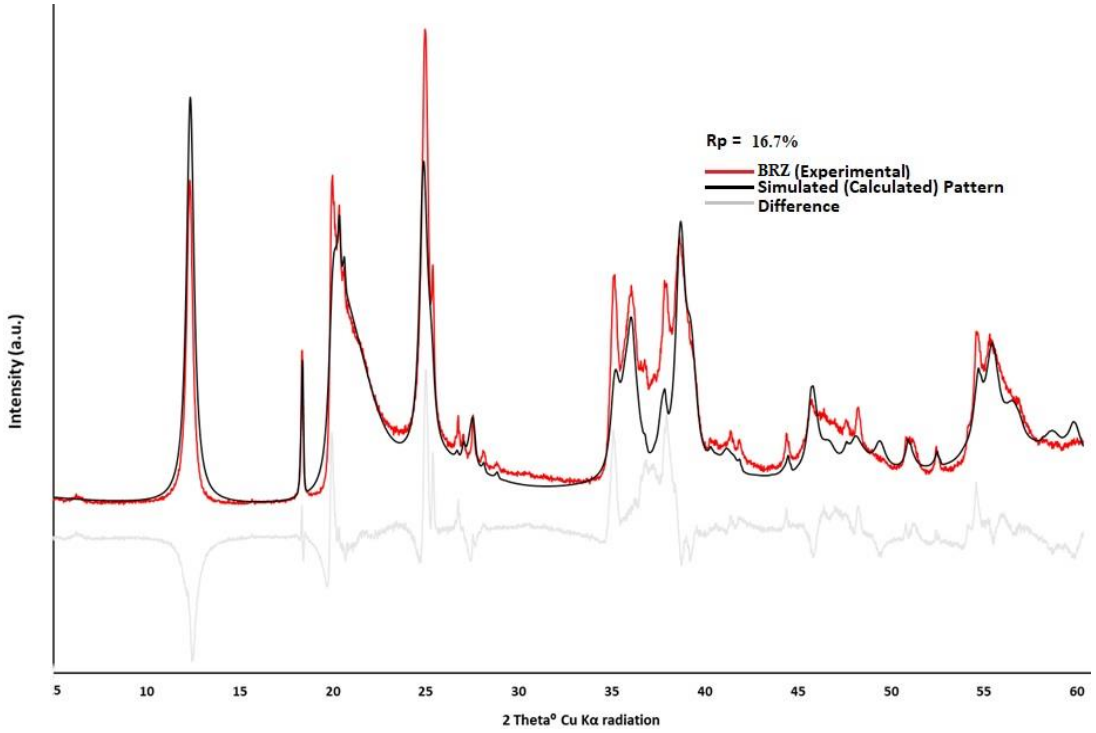

Figure 37 Experimental (red) and the calculated XRD (black) patterns of BRZ

Table 3. Structural parameters used in the refinement of BRZ.

Displacement Vectors			
	$\vec{t}_1$	$\vec{t}_2$	$\vec{t}_0$
P(%)	45	35	20

Unit Cell Parameters				
	a (Å)	b (Å)	c* (Å)	γ (deg)
Initial	5.1554	8.9448	7.1557	89.82
Final	5.1554	8.9448	7.1900	89.96

4.5.3 WAI

Just as in the case of BRZ, accessory minerals were first quantified by Rietveld refinement and used as background files in FAULTS. Just as in BRZ, the best agreement between the experimental and calculated pattern was arrived at when taken in proportion 45%, 35% and 20%, $\vec{t}_1$, $\vec{t}_2$, and $\vec{t}_0$, respectively, at Rp = 20.82% (Figure 38). The WAI sample is highly disordered and contains a single phase just as the BRZ sample. The high Rp values for both BRZ and WAI samples are likely due to the presence of many accessory and amorphous phases. Amorphous phases were not quantified in both cases. The unit cell parameters of for WAI is as presented in Table 4.

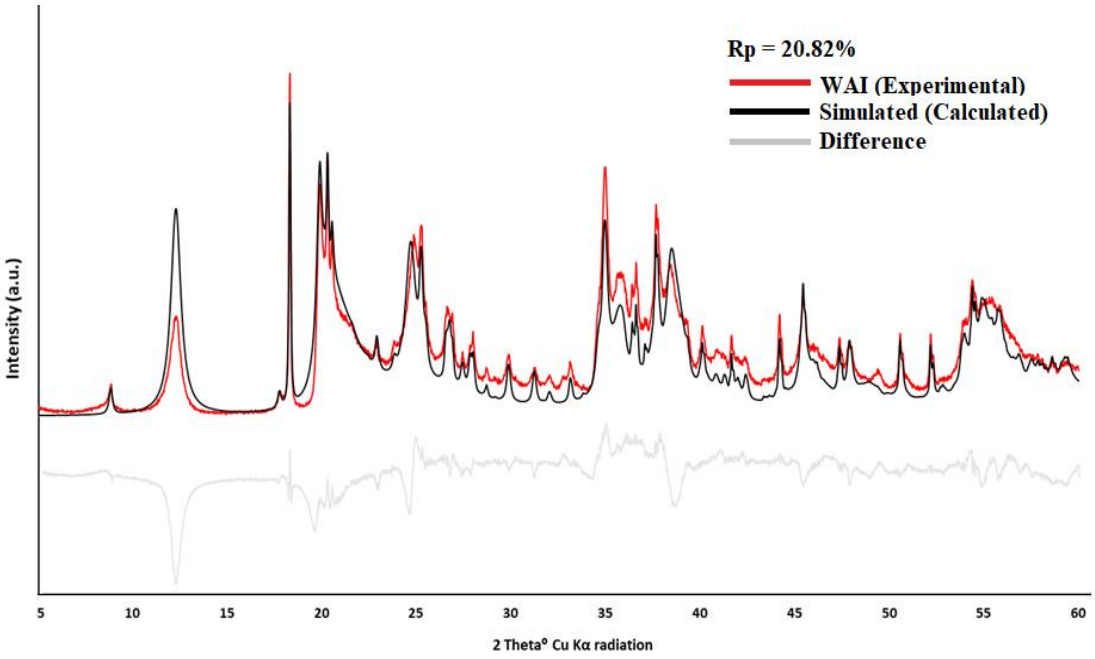

Figure 38 Experimental (red) and the calculated XRD (black) patterns of WAI

Table 4. Structural parameters used in the refinement of WAI.

Displacement Vectors			
	$\vec{t}_1$	$\vec{t}_2$	$\vec{t}_0$
P(%)	45	35	20

Unit Cell Parameters				
	a (Å)	b (Å)	c* (Å)	γ (deg)
Initial	5.1554	8.9448	7.1557	89.82
Final	5.1642	8.9626	7.2167	90.00

4.6 Thermal Stability

The acquired patterns at each stage of the thermal stability experiment (earlier described in section 3.8.1) is as shown in Figures 39, 40 and 41 for KGa BRZ and WAI, respectively. To investigate if the degree of disorder in kaolinite affects thermal stability, the dehydroxylation of the samples (extrapolated from the height of the *001* reflection) at each stage of heating was monitored. In the least disordered sample (KGa) the *001* reflection did not completely disappear up till 550 °C while in the highly disordered soil kaolinites (BRZ and WAI), complete dehydroxylation of the samples (disappearance of the *001* reflection) was at 500 °C. Thus, the least disordered sample was the most thermally stable of the three studied samples.

It was not possible to infer thermal stability between BRZ and WAI from the XRD patterns since both sample were completely dehydroxylated at the same temperature. A way around this challenge was to monitor the rate of the dehydroxylation from a graph of the ratio of H_T and H_{30} vs Temperature (Figure 42), where H_T is the height of the *001* reflection at a given temperature T while H_{30} is the height of the *001* reflection at 30 °C. The concavity of the plots is an indication of the resilience of the given sample to dehydroxylation. The KGa plot was the most concave, followed by BRZ and least was WAI. The resilience to dehydroxylation seem to decrease with increasing disorder within the structure of the considered kaolinite samples.

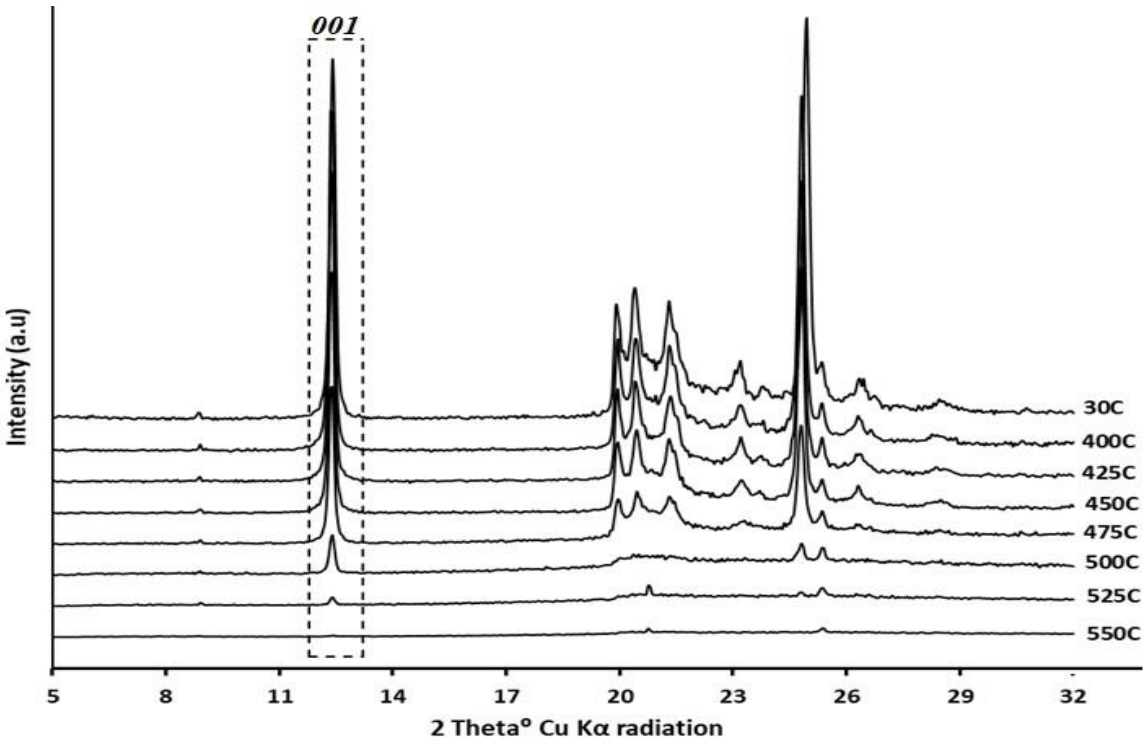

Figure 39 XRD patterns of KGa at various temperatures

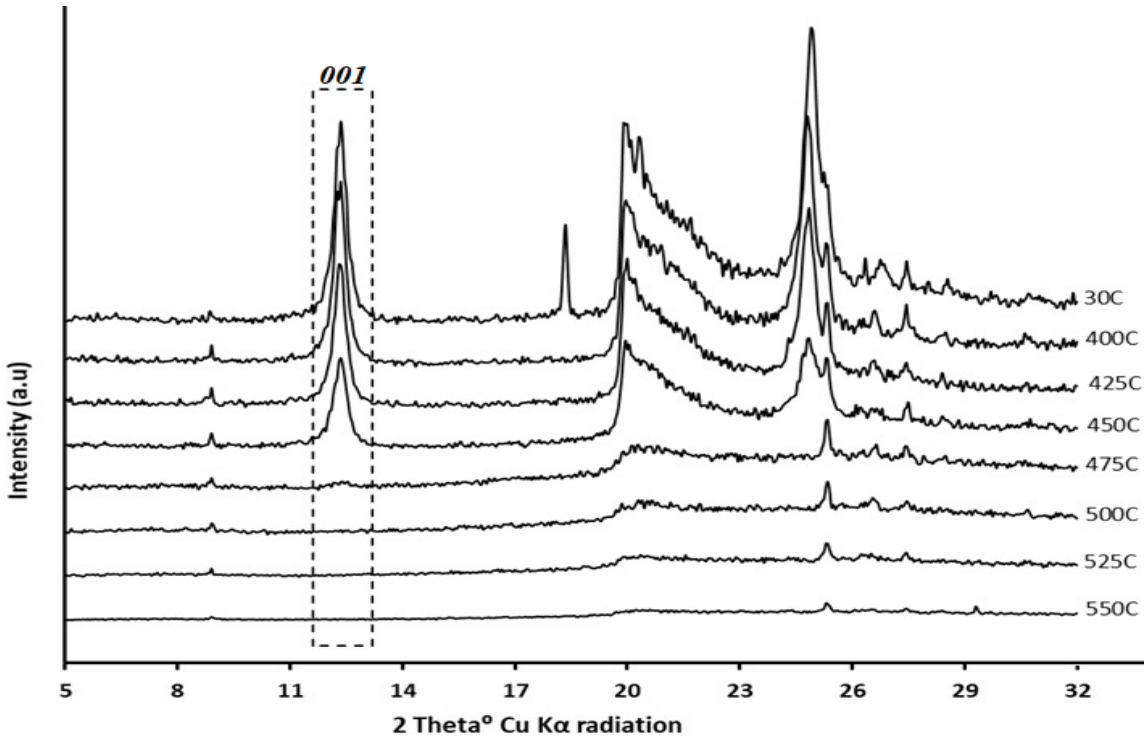

Figure 40 XRD patterns of BRZ at various temperatures

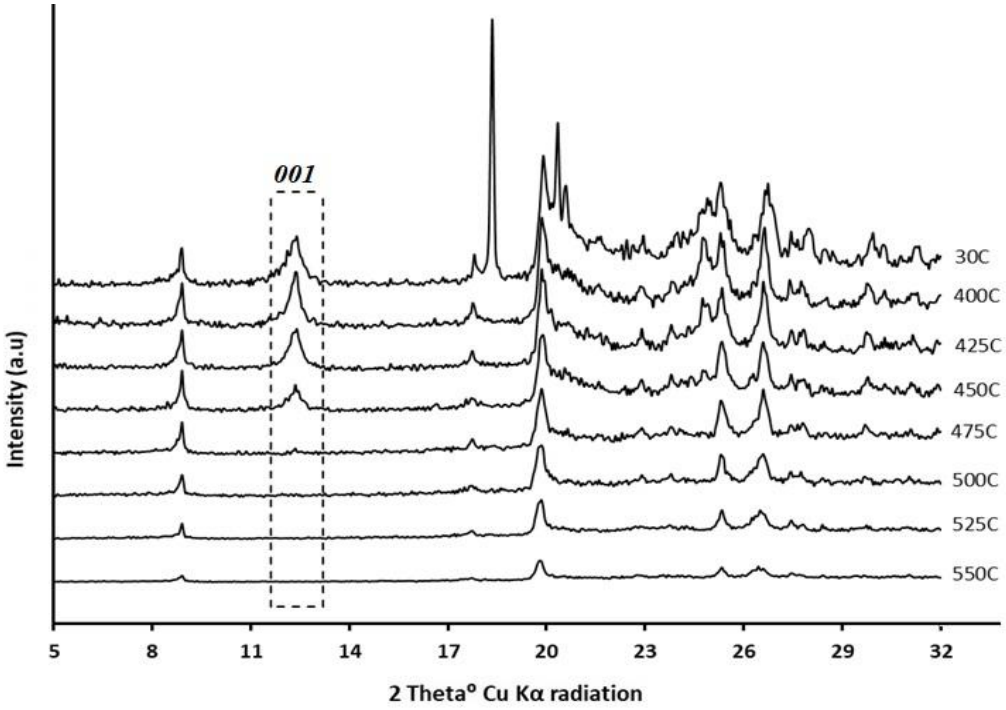

Figure 41 XRD patterns of WAI at various temperatures

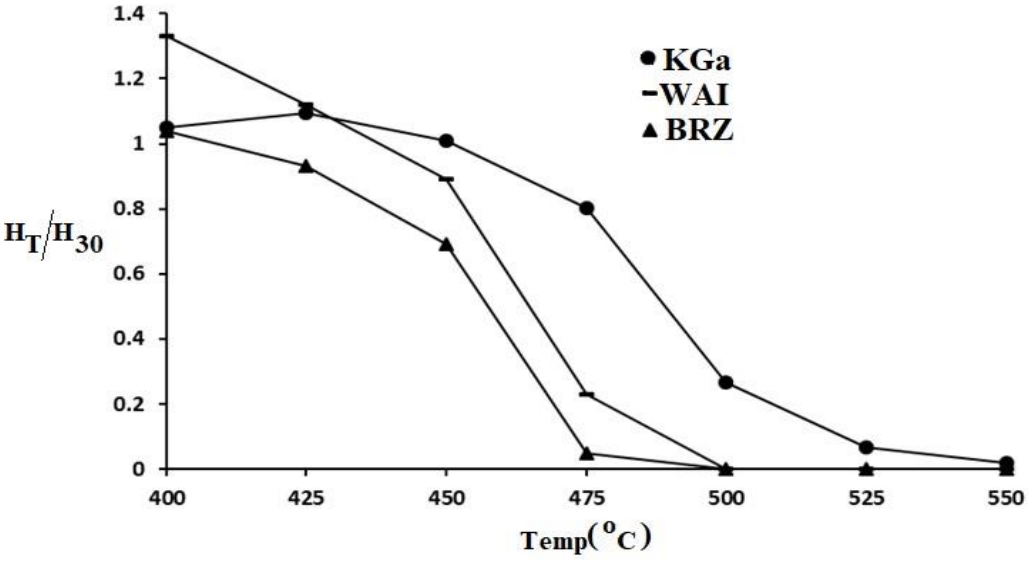

Figure 42 Graph of the ratio of H_T and H_{30} vs Temperature. Where H_T is the height of the *001* reflection at a given temperature T while H_{30} is the height of the *001* reflection at 30 °C

5. SUMMARY AND CONCLUSIONS

In this study, stacking disordering in kaolinite was studied using three samples - one geologic and two pedogenic specimens - by modeling of XRD diffraction patterns based on models described in previous literature.

There were differences in the modeled patterns of the geologic specimen compared to the soil specimens. The first been that the geologic sample contains two kaolinite phases while the soil specimen contained just a single kaolinite phase. Stacking disorder was more abundant in the soil specimens as evident in the high interstratification of $\vec{t}_1$ and $\vec{t}_2$ translation vectors. The $\vec{t}_0$ translation vector was very low in the geologic specimen, but this value was high as 20% in the soil specimens. The high $\vec{t}_0$ proportion value was necessary to reproduce the smearing of the reflections observed at higher angles in the soil specimens.

To achieve a good fit between the experimental and calculated XRD patterns for the soil specimens, influence of accessory minerals on the experimental XRD patterns was eliminated. The first approach was by thermal destruction and subtraction of accessory minerals. This approach was not successful due to the presence of amorphous phases left behind after destruction of the target accessory mineral. A second approach was to quantify the accessory minerals by Rietveld refinement. By this method it was possible to quantify the accessory minerals and block their reflections from experimental XRD pattern of the soil specimens.

The goodness of fit of the modeled XRD patterns of the soil specimens were higher despite efforts to mask the influence of other accessory phases (e.g. gibbsite). The high Rp values were probably due to the influence of crystalline and amorphous (not quantified or blocked) phases in the soil specimen samples. Another plausible reason for the lack of a very good agreement between the experimental and the modeled XRD pattern for the soil specimens is preferential orientation. Unlike the geologic specimen, the soil samples were not spray-dried because of the small quantity of the soil specimens. To achieve a good fit for the soil specimens in the future, it will be necessary to reduce preferential orientation by spray-drying the samples. In addition to spray-drying, the amorphous phases should be quantified preferably by mixing the samples with known quantity of an 100% crystalline mineral (which serves as an internal standard) prior to Rietveld refinement.

The thermal stability experiment showed that the least disordered sample (the geologic kaolinite) was more stable to dehydroxylation compared to soil kaolinite. The two soil kaolinites exhibited similar dehydroxylation behavior.

REFERENCES

Adams, J. M. (1983). Hydrogen atom positions in kaolinite by neutron profile refinement. *Clays and Clay Minerals*, *31*(5), 352–356.

Akiba, E., Hayakawa, H., Hayashi, S., Miyawaki, R., Tomura, S., Shibasaki, Y., … 1. (1997). Structure Refinement of Synthetic Deuterated Kaolinite by Rietveld Analysis Using Time-of-Flight Neutron Powder Diffraction Data. *Clays and Clay Minerals*, *45*(6), 781–788. https://doi.org/10.1346/CCMN.1997.0450602

Alves, M. E., Mascarenhas, Y. P., French, D. H., & Vaz, C. P. M. (2007). Rietveld-based mineralogical quantitation of deferrified oxisol clays. *Soil Research*, *45*(3), 224–232.

Aparicio, P., Ferrell, R. E., & Galán, E. (1999). A new kaolinite crystallinity index from mathematical modelling of XRD data. In *Abstracts volume of the 9 th EUROCLAY Conference* (p. 57).

Aparicio, P., & Galan, E. (1999). Mineralogical interference on kaolinite crystallinity index measurements. *Clays and Clay Minerals and Ctay Minerals*, *47*(I), 12–27.

Artioli, G., Bellotto, M., Gualtieri, A., & Pavese, A. A. (1995). Nature of structural disorder in natural kaolinites: a new model based on computer simulation of powder diffraction data and electrostatic energy calculation. *Clays and Clay Minerals*, *43*(4), 438–445.

Bailey, S. W. (1963). Polymorphism of the kaolin minerals. *American Mineralogist: Journal of Earth and Planetary Materials*, *48*(11–12), 1196–1209.

Bailey, S. W. (1980). Structures of layer silicates. In G. Wi. Brindley & G. Brown (Eds.), *Crystal Structures of Clay Minerals and the X-ray Identification* (pp. 1–123). Mineral. Soc.

Bates, T. F. (1971). The kaolin minerals. In J. Gard (Ed.), *The Electron-Optical Investigation of Clays* (Vol. 3, pp. 109–157).

Baur, W. H. (1965). On hydrogen bonds in crystalline hydrates. *Acta Crystallographica*, *19*(6), 909–916. https://doi.org/10.1107/S0365110X65004632

Ben Rhaiem, H. (1999). *Analyse multiéchelle de phyllosilicates tunisiens par diffraction aux petits angles des RX et par MET. Relation entre structure, microtexture et propriétés macroscopiques d'hydratation au cours d'un cycle de dessication-humectation*. Th{è}se d'Etat de l'Universit{é} de Tunis II.

Bergaya, F., Lagaly, G., & Vayer, M. (2006). Cation and Anion Exchange. *Developments in Clay Science*, *1*, 979–1001.

Bish, D. L. (1993). Rietveld Refinement of the Kaolinite Structure at 1.5 K. *Clays and Clay Minerals*, *41*(6), 738–744.

Bish, D. L. (1994). Quantitative X-ray diffraction analysis of soils. *Quantitative Methods in Soil Mineralogy*, (quantitativemet), 267–295.

Bish, D. L., & Post, J. E. (1993). Quantitative mineralogical analysis using the Rietveld full-pattern fitting method. *American Mineralogist*, *78*(9–10), 932–940.

Bish, D. L., & Von Dreele, R. B. (1989). Rietveld Refinement of Non-Hydrogen Atomic Positions in Kaolinite. *Clays and Clay Minerals*, *37*(4), 289–296.

Bookin, A. S., Drits, V. A., Plançon, A., & Tchoubar, C. (1989). Stacking faults in

kaolin-group minerals in the light of real structural features. *Clays and Clay Minerals*, *37*(4), 297–307.

Braggs, B., Fornasiero, D., Ralston, J., Smart, R. S., & others. (1994). The effect of surface modification by an organosilane on the electrochemical properties of kaolinite. *Clays and Clay Minerals*, *42*(2), 123–136.

Brinatti, A. M., Mascarenhas, Y. P., Pereira, V. P., Partiti, C. S. de M., & Macedo, Á. (2010). Mineralogical characterization of a highly-weathered soil by the Rietveld Method. *Scientia Agricola*, *67*(4), 454–464.

Brindley, G. W. (1961). Kaolin, serpentine, and kindred minerals. In *X-ray Identification and Crystal Structures of Clay Minerals. Mineralogical Society of London* (pp. 51–131).

Brindley, G. W. (1980). Order-Disorder in Clay Minerals. In G. W. Brindley & G. Brown (Eds.), *Crystal Structure of Clay Minerals and their X-ray Identification, Mineralogical Society, London* (pp. 125–196).

Brindley, G. W., & Robinson, K. (1946). The structure of kaolinite. *Mineralogical Magazine*, *27*(194), 242–253. Retrieved from http://www.minersoc.org/pages/Archive-MM/Volume_27/27-194-242.pdf

Casas-Cabanas, M., Reynaud, M., Rikarte, J., Horbach, P., Rodríguez-Carvajal, J., D., B., … de, W. P. M. (2016). FAULT : a program for refinement of structures with extended defects. *Journal of Applied Crystallography*, *49*(6), 2259–2269. https://doi.org/10.1107/S1600576716014473

Chàvez, G. L., & Johns, W. D. (1995). Mineralogical and ceramic properties of

refractory clays from central Missouri (USA). *Applied Clay Science*, *9*(6), 407–424. https://doi.org/10.1016/0169-1317(95)00004-N

Coelho, A. A. (2005). TOPAS-Academic, Version 5. *Brisbane, Australia*.

Collins, D. R., & Catlow, C. R. A. (1991). Energy-minimized hydrogen-atom positions of kaolinite. *Acta Crystallographica Section B Structural Science*, *47*(5), 678–682. https://doi.org/10.1107/S010876819100561X

Davis, D. W. (1950). *Electron micrographs of reference clay minerals*. Columbia University.

Delarmelinda, E. A., de Souza Júnior, V. S., Wadt, P. G. S., Deng, Y., Campos, M. C. C., & Câmara, E. R. G. (2017). Soil-landscape relationship in a chronosequence of the middle Madeira River in southwestern Amazon, Brazil. *Catena*, *149*, 199–208.

DeLuca, S., & Slaughter, M. (1985). Existance of multiple kaolinite phases and their relationship to disorder in kaolin minerals. *American Mineralogist*, *70*, 149–158.

Deng, Y., White, G. N., & Dixon, J. B. (2013). Soil mineralogy laboratory manual. *Department of Soil and Crop Sciences. Texas A &M University, College Station, Texas*, 77843–82474.

Dixon, J. B. (1989). Kaolin and serpentine group minerals. *Minerals in Soil Environments*, (mineralsinsoile), 467–525.

Doebelin, N., & Kleeberg, R. (2015). Profex: a graphical user interface for the Rietveld refinement program BGMN. *Journal of Applied Crystallography*, *48*(5), 1573–1580.

Drits, V. A., & Tchoubar, C. (1990). *X-Ray Diffraction by Disordered Lamellar*

Structures: Theory and Applications to Microdivided Silicates ans Carbons. *Springer-Verlag*.

Giese, R. F. (1988). Kaolin Minerals: Structures and Stabilities. In B. S. W (Ed.), *Hydrous Phyllosilicates (Exclusive of Micas)* (Vol. 19, pp. 29–66). Reviews in Mineralogy and Geochemistry. Mineralogical Society of America.

Gilkes, R. J., & Prakongkep, N. (2016). How the unique properties of soil kaolin affect the fertility of tropical soils. *Applied Clay Science*, *131*, 100–106. https://doi.org/10.1016/j.clay.2016.01.007

Gruner, J. W. (1932). The Crystal Structure of Kaolinite. *Zeitschrift Für Kristallographie - Crystalline Materials*, *83*(1–6), 75–88. https://doi.org/doi:10.1524/zkri.1932.83.1.75

Guggenheim, S., Alietti, A., Bain, D. C., Drits, V. A., Formoso, M. L. L., Galan, E., … Wantanbe, T. (1997). Report of the Association Internationale Pour l'Etude des Argiles (Aipea) Nomenclature Committee for 1996. *Clays and Clay Minerals*, *45*(2), 298–300. https://doi.org/10.1346/CCMN.1997.0450219

Guinier, A. (1964). *Théorie et technique de la radiocristallographie*.

Hart, R. D., Gilkes, R. J., Siradz, S., & Singh, B. (2002). The nature of soil kaolins from Indonesia and Western Australia. *Clays and Clay Minerals*, *50*(2), 198–207.

Hendricks, S. B. (1936). Concerning the Crystal Structure of Kaolinite, Al2O3. 2SiO2 .2H2O, and the Composition of Anauxite. *Zeitschrift Für Kristallographie - Crystalline Materials*, *95*(1–6), 509–518.

Hendricks, S., & Teller, E. (1942). X-Ray Interference in Partially Ordered Layer

Lattices. *The Journal of Chemical Physics*, *10*(3), 147–167.

Hillier, S. (1999). Use of an air brush to spray dry samples for X-ray powder diffraction. *Clay Minerals*, *34*(1), 127–135.

Hinckley, D. N. (1962). Variability an “crystallinity” values among the koalin deposits of the coastal plain of Georgia and South Carolina. *Clays and Clay Minerals*, *11*(1), 229–235. https://doi.org/10.1346/CCMN.1962.0110122

Hughes, J. C., & Brown, G. (1979). A crystallinity index for soil kaolins and its relation to parent rock, climate and soil maturity. *European Journal of Soil Science*, *30*(3), 557–563.

Hughes, J. C., Gilkes, R. J., & Hart, R. D. (2009). Intercalation of reference and soil kaolins in relation to physico-chemical and structural properties. *Applied Clay Science*, *45*(1), 24–35.

Johnston, C. T., Kogel, J. E., Bish, D. L., Kogure, T., & Murray, H. H. (2008). Low-temperature Ftir Study of Kaolin-Group Minerals. *Clays and Clay Minerals*, *56*(4), 470–485. Retrieved from http://dx.doi.org/10.1346/CCMN.2008.0560408

Kogure, T. (2011). Stacking disorder in kaolinite revealed by HRTEM: a review. *Clay Science*, *15*(1), 3–11.

Kogure, T., Elzea-Kogel, J., Johnston, C. T., & Bish, D. L. (2010). Stacking Disorder in a Sedimentary Kaolinite. *Clays and Clay Minerals*, *58*(1), 62–71. https://doi.org/10.1346/CCMN.2010.0580106

Kogure, T., & Inoue, A. (2005). Determination of defect structures in kaolin minerals by high-resolution transmission electron microscopy (HRTEM). *American*

Mineralogist, *90*(1).

Ladd, M. F. C. (1968). The location of hydrogen atoms in crystalline ionic hydrates, *126*, 147–152. Retrieved from http://citeseerx.ist.psu.edu/viewdoc/download?doi=10.1.1.526.3446&rep=rep1&type=pdf

Ledoux, R. L., & White, J. L. (1964). Infrared study of the OH groups in expanded kaolinite. *Science (New York, N.Y.)*, *143*(3603), 244–246. https://doi.org/10.1126/SCIENCE.143.3603.244

Lee, S. Y., Jackson, M. L., & Brown, J. L. (1975). Micaceous occlusions in kaolinite observed by ultramicrotomy and high resolution electron microscopy. *Clays and Clay Minerals*, *23*(2), 125–129.

Lim, C. H., Jackson, M. L., Koons, R. D., & Helmke, P. A. (1980). Kaolins: Sources of differences in cation-exchange capacities and cesium retention. *Clays and Clay Minerals*, *28*(3), 223–229.

Ma, C., & Eggleton, R. A. (1999). Surface layer types of kaolinite: a high-resolution transmission electron microscope study. *Clays and Clay Minerals*, *47*(2), 181–191.

Meads, R. E., & Malden, P. J. (1975). Electron spin resonance in natural kaolinites containing Fe (super 3+) and other transition metal ions. *Clay Minerals*, *10*, 313–345.

Mehra, O. P., & Jackson, M. L. (1960). Iron oxide removal from soils and clays by a dithionite--citrate system buffered with sodium bicarbonate. In *Clays and clay minerals: proceedings of the Seventh National Conference* (pp. 317–327).

Melo, V. F., Singh, B., Schaefer, C., Novais, R. F., & Fontes, M. P. F. (2001). Chemical and mineralogical properties of kaolinite-rich Brazilian soils. *Soil Science Society of America Journal*, *65*(4), 1324–1333.

Mestdagh, M. M., Vielvoye, L., & Herbillon, A. J. (1980). Iron in kaolinite: II. The relationship between kaolinite crystallinity and iron content. *Clay Minerals*, *15*(1), 1–13.

Murray, H. (1954). Structural variations of some kaolinites in relation to dehydrated halloysite. *American Mineralogist*, *39*(1), 97–108.

Murray, H. H. (1991). Overview — clay mineral applications. *Applied Clay Science*, *5*(5–6), 379–395.

Murray, H. H. (2006). Chapter 5 Kaolin Applications. In *Applied Clay Mineralogy Occurrences, Processing and Application of Kaolins, Bentonites, Palygorskite-Sepiolite, and Common Clays* (pp. 85–109). https://doi.org/10.1016/S1572-4352(06)02005-8

Neder, R. B., Burghammer, M., Grasl, T., Schulz, H., Bram, A., & Fiedler, A. S. (1999). Refinement of the kaolinite structure from single-crystal synchrotron data. *Clays and Clay Minerals*, *47*(4), 487–494.

Newman, A. C. D., & Brown, G. (1987). The Chemical Constitution of Clays. In A. C. D. Newman (Ed.), *Chemistry of clays and clay minerals (Mineralogical Society Monograph, No 6)* (pp. 1–128). John Wiley & Sons, New York.

Pierre, T. G. S., Singh, B., Webb, J., & Gilkes, B. (1992). Mossbauer spectra of soil kaolins from south-western Australia. In *Clays Clay Miner*.

Plançon, A., Giese Jr, R. F., Snyder, R., Drits, V. A., & Bookin, A. S. (1989). Stacking faults in the kaolin-group minerals: Defect structures of kaolinite. *Clays and Clay Minerals*, *37*(3), 203–210.

Plançon, A., Giese, R. F., & Snyder, R. (1988). Hinckley index for kaolinites. *Clays and Clay Minerals*, *23*(3), 249–260.

Plançon, A., & Tchoubar, C. (1975). Etude des fautes d'empilement dans les kaolinites partiellement désordonnées. I. Modèle d'empilement ne comportant que des fautes de translation. *Journal of Applied Crystallography*, *8*(6), 582–588.

Plançon, A., & Tchoubar, C. (1976). Etude des fautes d'empilement dans les kaolinites partiellement désordonnées. II. Modèles d'empilement comportant des fautes par rotation. *Journal of Applied Crystallography*, *9*(4), 279–285.

Plançon, A., & Tchoubar, C. (1977a). Determination of Structural Defects in Phyllosilicates by X-Ray Powder Diffraction---II. Nature and Proportion of Defects in Natural Kaolinites. *Clays and Clay Minerals*, *25*, 436–450.

Plançon, A., & Tchoubar, C. (1977b). Determination of structural defects in phyllosilicates by X-ray powder diffraction; I, Principle of calculation of the diffraction phenomenon. *Clays and Clay Minerals*, *25*(6), 430–435.

Plancon, A., & Zacharie, C. (1990). An expert system for the structural characterization of kaolinites. *Clay Minerals*, *25*, 249–260.

Range, K. J., Range, A., & Weiss, A. (1969). Fire-clay type kaolinite or fire-clay mineral? Experimental classification of kaolinite-halloysite minerals. In *International Clay Conference* (pp. 3–11). Tokyo: Israel University Press

Jerusalem.

Rietveld, H. (1969). A profile refinement method for nuclear and magnetic structures. *Journal of Applied Crystallography*, *2*(2), 65–71.

Rietveld, H. M. (1967). Line profiles of neutron powder-diffraction peaks for structure refinement. *Acta Crystallographica*, *22*(1), 151–152.

Ruiz Cruz, M. D. (1994). Diagenetic Development of Clay and Related Minerals in Deep Water Sandstones (S. Spain): Evidence of Lithological Control. *Clay Minerals*, *29*(1), 93–104. https://doi.org/10.1180/claymin.1994.029.1.11

Rushbrooke, G. S. (1949). *Introduction to statistical mechanics*. The Clarendon Press, Oxford.

Sakharov, B. A., Drits, V. A., McCarty, D. K., & Walker, G. M. (2016). Modeling Powder X-Ray Diffraction Patterns of the Clay Minerals Society Kaolinite Standards: Kga-1, Kga-1b, and Kga-2. *Clays and Clay Minerals*, *64*(3), 314–333.

Samotoin, N. D. (1966). Study of surface of kaolinite and dickite monocrystals by decoration method. *Zap. Vses. Mineral. Obshch*, (95), 390–399.

Serratosa, J. M., Hidalgo, A., & Vinas, J. M. (1963). Infrared study of the OH groups in kaolin minerals. In *Proceedings of the conference held at Stockholm, Sweden, August 12-16* (Vol. 1, p. 17).

Singh, B., & Gilkes, R. J. (1992). Properties of soil kaolinites from south-western Australia. *European Journal of Soil Science*, *43*(4), 645–667.

Siradz, S. A. (2002). *Mineralogy and chemistry of red soils of Indonesia*. University of Western Australia.

Smith, S. T., Snyder, R. L., & Brownell, W. E. (1978). Minimization of preferred orientation in powders by spray-drying. *Adv. X-Ray Anal. 22, 77, 1978*.

Soukup, D. A., Buck, B. J., & Harris, W. (2008). Preparing Soils for Mineralogical Analyses. In *Methods of Soil Analysis Part 5—Mineralogical Methods* (pp. 13–31). Madison, WI: Soil Science Society of America. https://doi.org/10.2136/sssabookser5.5.c2

Stoch, L. (1974). *Minera{\l}y ilaste*. Wydawnictwa Geologiczne.

Stucki, J. W. (2006). Properties and behaviour of iron in clay minerals. *Developments in Clay Science*, *1*, 423–475.

Taylor, J. C. (1991). Computer programs for standardless quantitative analysis of minerals using the full powder diffraction profile. *Powder Diffraction*, *6*(1), 2–9.

Tchoubar, C., Plancon, A., Ben Brahim, J., Clinard, C., & Sow, C. (1982). Caract{é}ristiques structurales des kaolinites d{é}sordonn{é}es. *Bulletin de Min{é}ralogie*, *105*, 477–491.

Thompson, J. G., & Cuff, C. (1985). Crystal structure of kaolinite: dimethylsulfoxide intercalate. *Clays and Clay Minerals*, *33*(6), 490–500.

Thompson, P., Cox, D. E., & Hastings, J. B. (1987). Rietveld Refinement of Debye-Scherrer Synchrotron X-ray Data from A1203. *J. Appl. Cryst*, *20*, 79–83. Retrieved from https://journals.iucr.org/j/issues/1987/02/00/a27720/a27720.pdf

Treacy, M. M. J., Deem, M. W., & Newsam, J. M. (2010). How DIFFaX Works (pp. 42–48). Retrieved from http://www.public.asu.edu/~mtreacy/DIFFaX_manual.pdf

Varajão, A. F. D. C., Gilkes, R. J., & Hart, R. D. (2001). The relationships between

kaolinite crystal properties and the origin of materials for a Brazilian kaolin deposit. *Clays and Clay Minerals*, *49*(1), 44–59.

Veblen, D. R. (1985). Direct TEM imaging of complex structures and defects in silicates. *Ann. Rev. Earth Planet. Sci*, *13*, 119–46.

Velho, J., & de SF Gomes, C. (1991). Characterization of Portuguese kaolins for the paper industry: beneficiation through new delamination techniques. *Applied Clay Science*, *6*(2), 155–170.

Weaver, C. E. (1976). The nature of TiO2 in in kaolinite. *Clays and Clay Minerals*, *24*, 215–218.

White, G. N., & Dixon, J. B. (2002). Kaolin-serpentine minerals. In *Soil mineralogy with environmental applications* (pp. 389–414). Soil Science Society of America.

Wilson, M. J., Deer, W. A., Howie, R. A., & Zussman, J. (2013). Kaolin Clay Minerals. In M. J. Wilson (Ed.), *Rock-Forming Minerals, Volume 3C, Sheet Silicates: Clay Minerals* (pp. 33–77). Geological Society, London.

Wolf, R. G. (1963). Structural Aspects of Kaolinite Using Infrared Absorption. *The American Mineralogist*, *48*, 390–399.

Young, R. A., & Hewat, A. A. W. (1988). Verification of the Triclinic Crystal Structure of Kaolinite. *Clays and Clay Minerals*, *36*(3), 225–232.

Zabala, M. S., Conconi, M. S., Alconada, M., Torres, R. M., & Sanchez, R. M. (2007). The Rietveld method applied to the quantitative mineralogical analysis of some soil samples from Argentina. *Revista Cienciadel Suelo*, *25*, 65–73.

Zvyagin, B. B., & Drits, V. A. (1996). Interrelated features of structure and stacking of

kaolin mineral layers. *Clays and Clay Minerals*, *44*(3), 297–303.